Synthesis of poly(methyl methacrylate-co-methacrylic acid) copolymers and their application in the development of oral and transdermal drug delivery systems

by

Harish Chakrapani

A thesis submitted in partial fulfillment of the requirements for the degree of

Master of Science

in

Chemical Engineering

Department of Chemical and Materials Engineering
University of Alberta

Abstract

pH-responsive polymers have been intensively investigated over the years due to their diverse applications in environmental decontamination, nutrient delivery/packaging, cosmetics, and pharmaceutical science. A pH-responsive swelling/shrinkage behavior of encapsulation systems can be accounted for by the conformation change of polymer chains at different pH. However, it is unusual to find their commercial applications due to several technical limitations such as incomplete protection of the encapsulated ingredients against harsh environmental conditions, weak response to pH change, and inefficient release behavior. Previously in our group, macropored microparticles (MPs) have been developed to increase drug loading capacities and protect the drugs from harsh gastric environments using commercially available pH responsive polymers, overcoming major technical challenges for oral drug delivery systems. We wanted to further synthesize copolymers with different material properties such as pKa, (acid dissociation constants) by changing the hydrophobic/hydrophilic ratio of methyl methacrylate to methacrylic acid to better understand the effects of pH responsiveness and their influence on pH responsive drug delivery system to overcome the fixed characteristics of commercially available polymers.

To this end, we synthesized pH-responsive low molecular weight poly (methyl methacrylate-co-methacrylic acid) copolymer with different acid dissociation constants for better intestinal targeting using free radical solvent copolymerization. We further characterized the copolymers and used them to fabricate MPs with pH-responsive macropores in the development of intestine-targeted oral drug delivery systems. The pH-responding release behaviour of the pored MPs was examined by monitoring time-dependent release profile of encapsulated 100-nm fluorescent nanoparticles in simulated gastrointestinal (GI) tract environment. Further we

encapsulated pH-sensitive drug and measured the remaining activity after subjected to GI tract. Our pH-sensing copolymer and MP delivery system will advance the current microencapsulation technology by solving key challenges in encapsulation, protection, and release of oral drugs and biopharmaceuticals.

Another important characteristic of these anionic copolymers is their environmental stability. They can be used as protective layers for long-term storage stability as these polymers can protect the drugs from moisture. Microneedles have been researched extensively as an effective drug delivery system for transdermal applications. However, due to low mechanical strength of the conventional based sugar microneedles, it is difficult for them to penetrate the animal skin. Moreover, these sugar-based microneedles are not environmentally stable, failing to protect the drugs from moisture. In this work, we used micromolding techniques to fabricate cellulose nanocrystal-based microneedles of different concentrations and studied the mechanical strength of the microneedles. The microneedles fabricated by cellulose nanocrystals (CNC) and trehalose formulations had almost 6-fold increase in the failure force of the microneedles than the previously fabricated microneedles with CMC and trehalose formulations. Also, we coated these CNC-trehalose based microneedles with the anionic copolymer, i.e. Eudragit S100, by custom designed spray coating device to increase the long-term storage stabilities. Our CNC microneedles will advance the current sugar-based microneedles with higher mechanical strength and greater drug stability and would be the future way of delivering vaccines over conventional needle injections.

Acknowledgement

I would like to express my deepest appreciation and gratitude to Dr. Joao Soares and Dr. Hyo-Jick Choi, my supervisors for providing me constant support and inspiring me to be the person I am today. Dr. Joao Soares always believed my capabilities in achieving something unique. His cool attitude towards life has taught me how to approach problems in a different way. Whenever, I lacked motivation or had any sort of bad day, he has always been my support in encouraging me and putting things on right track. He has always encouraged me even when I was failing in my experiments showing the level of confidence, he had in me as an experimentalist.

Dr. Hyo-Jick Choi, has been like a pillar to me for his constant guidance every time. He not only supervised me, but also worked along with me and had always been curious about the experiments in the lab, every single day. Thanks to his open criticism, which made me a better researcher in terms of thinking, planning and execution of experiments and meeting all requirements required to develop myself as a professional individual. He personally made lots of efforts in teaching me all the required skills to become professional scientist. No matter, what degree we pursued (Masters/ PhD), he has shown similar respect towards everyone in the group as a scientist, which boosted everyone's confidence and made everyone work smart in creating and implementing new ideas. Furthermore, he has always helped me to develop my career which is the best qualities a supervisor can do.

I would like to thank my colleague, Dr. Surjith Kumaran for his help in all regards personally and scientifically in conducting experiments, installing gas lines, in building the spray coating system, and lots more. I would also like to thank all my group members Matthew Lawson (coffee

Table of contents

List of figures

List of tables

List of Abbreviations

MMA: Methyl Methacrylate

MAA: Methacrylic acid

DCM: Dichloromethane

IPA: Isopropanol

MPs: Microparticles

MNs: Microneedles

GI: Gastrointestinal

FNPs: Fluorescent Nanoparticles

SGF: Simulated Gastric Fluid

SIF: Simulated Intestinal Fluid

SEM: Scanning Electron Microscopy

DI: Deionized water

AIBN: 2,2'- Azobis-(2-methyl-propionitrl)

BCA: Bicinchoninic Acid

1. INTRODUCTION

1.1. Drug delivery

Drug delivery is the mechanism of administering a pharmaceutical/biopharmaceutical product to achieve a therapeutic effect in humans/animals [1]. The design of a drug delivery system is mainly based on the physiochemical and pharmacokinetic properties of the drug [2]. Drug delivery systems mainly focus on releasing the drugs at a target location; hence the drug delivery system must be designed in such a way that they wouldn't get in contact with the host defence mechanism but should be specific in terms of delivery [3]. Ideally, drug delivery system should deliver exact proportion of drugs to a target at a specific rate and time to maximize the therapeutic effect of the drugs [3]. Drug delivery technologies modify the drug release profile, drug absorption and distribution for improving drug/biopharmaceuticals efficacy and safety along with consideration of patience convivence [4,5]. In general, there are different routes of drug administration into the body depending on the disease and therapeutic effect desired. Some of the common routes of administration include oral, topical, inhalation, transdermal and parenteral (injections) [6,7]. Many medications such as proteins, peptides, vaccines cannot be delivered without a proper delivery system through these routes because they might be susceptible to enzymatic degradation, unfavourable conditions or cannot be absorbed due to molecular size [8]. However, we can tailor the formulations, use biocompatible or biodegradable materials and overcome these barriers for delivery of drugs to specific sites.

1.2. Stimuli-responsive polymers for drug delivery

Stimuli-responsive polymers are certain types of polymers that respond with property-based conformational changes with the changes in external environments as shown in Figure 1.1 [46,47]. The stimuli to which the polymers react could be temperature, pH, ionic strength, light, electric or magnetic field [47]. These polymers are referred to as "smart polymers" and have been emerging due to their biomedical applications as in drug delivery carriers. Over the last few years, stimuli-responsive polymers have gained lots of attention for their biomedical applications [4,11]. Stimuli-responsive polymers show a sharp change in their properties when they come across a minute change in environmental conditions [5, 10]. These polymers can be used to synthesize smart drug delivery systems which could deliver drugs to targeted site based on the stimulated environmental conditions in our body or inducing it externally.
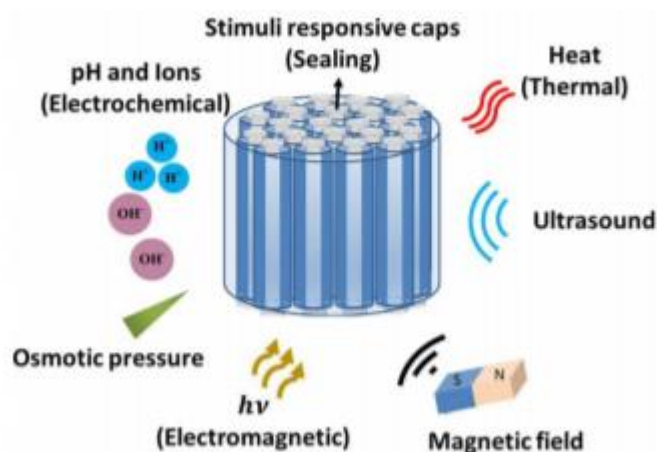
Figure 1.1. Stimuli responsive polymers – smart polymers under influence of different environmental conditions and their conformational changes [103]

1.3. Oral drug delivery:

Oral drug delivery is the most accepted forms of drug administration with advantages such as self-administration, ease, non-invasive nature and painless delivery of drugs compared to

hypodermal injections and other delivery routes [9]. However due to poor solubility, drug stability and bioavailability makes it challenging to achieve remedial effects through GI tract [9]. They have lots of barriers including pH gradients, especially acidic gastric environment and the mucus barrier which hinders drug absorption though having high absorption area (> 300 m^2) [9,60]. Therefore, one way to approach the problem is to tailor stimuli-responsive synthetic materials which could encapsulate drugs, delivering to the target site while keeping the drugs safe from the gastric environments. Synthetic polymers have emerged as a promising drug delivery carrier over the years due to their improved pharmacokinetics compared to other small molecule drugs with longer circulation time [10]. Over the years, there has been significant progress in developing oral delivery carriers using synthetic materials for efficient release and uptake of biopharmaceuticals [9]. The behaviour of the drug in GI tract is based on several factors such as pH, enzymes and other physiological aspects. Though there are several researches in improving the bioavailability of drugs to stabilise the active ingredients in GI tract, however, it failed to deliver drugs at the targeted site efficiently [49].

1.3.1. Oral influenza vaccine delivery

Vaccination is an effective and efficient way of preventing diseases [12, 32]. Most of the commercially available vaccines are administered through injections, with problems of safety and patient acceptability [30-32]. In recent years, due to advances in technology, needle-free vaccine delivery, among which oral, transdermal vaccine delivery have been extensively researched [33-35]. Among those, oral delivery of vaccines like any other drugs could also be self-administered without the need of a trained personnel [32]. Oral vaccine delivery is an essential prerequisite for increasing the immunity against most of the enteric as we all mucosal pathogens present in both

animals and humans [31]. However, for effective oral immunization, vaccine antigens should be protected from gastric environment and must be efficiently taken up by the GALT cells in the intestine, inducing immune response [32]. In 1918, the influenza outbreak infected about 500 million people of the earth's population [48], by the time it subsided in two years it has been estimated of about 50 million deaths [48]. There was another outbreak which almost killed one million people in 1957, initiated in China but spread globally [48]. Even in 2009, "Swine flu" A(H1N1) pandemic started in Mexico killed between 105,000 to 395,000 people [48]. It was predicted that treating a flu pandemic here on would cost 60 billion US dollars/year in contrast to 4.5 billion US dollars/year for vaccination and preventing the outbreak [48]. These pandemics are totally unpredictable. Moreover, the current vaccine production capacity is only 3 billion doses per year, substantially short of the 6.8 billion people who will be at risk of contracting influenza and spreading the virus [45]. Since the next outbreak is inevitable, it is an important to create efficient and cheap delivery carriers. Fortunately, vaccination can be the most effective strategy in preventing any such outbreaks.

1.3.2. pH sensitive polymeric microparticles

One of the main stimuli that can be used to release drugs when administered orally is associated with pH changes in the GI tract [18]. pH-responsive polymers due to their pH-induced ionization/deionization behavior can be used to protect the drugs/vaccines from the unfavourable conditions (stomach) and deliver it to targeted sites [18-19]. The change in pH along the GI tract from acidic (pH = 1-3) to basic in the intestine (pH = 5-8) could be considered for pH responsive drug delivery system for the drug of any kind [10]. pH-sensitive polymers can be broadly classified into anionic and cationic polymers, both having certain pKa (acid dissociation constant) values

[11]. These polymers are a class of polyelectrolytes having ionizable groups in their backbone, side or end group [11, 59]. Anionic pH-sensitive polymers are soluble at a pH higher than their pKa (e.g. sulphonic acid, carboxylic acid- which ionize at basic pH) [10]. Cationic pH-sensitive polymers are soluble at a pH lower than its pKa (e.g. Amino groups which ionize and dissolve at acidic pH) [11]. pH sensitiveness is determined by their characteristic structure of ionizing groups and can be modulated by several structural factors such as ionic strength, polymer composition, and hydrophobicity/hydrophilicity of the copolymer [11]. However, it is unusual to find their commercial applications due to several technical limitations such as incomplete protection of the encapsulated ingredients against harsh environmental conditions, weak response to pH change, and inefficient release behavior [16,25]. Hence, the drugs should be encapsulated into the smart delivery systems in order to overcome the challenges mentioned above.

Based on this background, polymeric MPs have been widely investigated as a potential delivery carrier in food, pharmaceutical and cosmetic industries due to their capability of encapsulating substances, protecting drug from unfavourable conditions [10, 12-16, 44]. There are several methods for synthesizing polymeric MPs such as phase separation, spray drying and emulsion-solvent evaporation to synthesize polymeric delivery carriers [16, 20-24]. Though these methods could be used to encapsulate hydrophilic and hydrophobic drugs along with microparticle formation, each of these methods have major disadvantages such as the use of organic solvents in case of phase separation and optimization of different variables (flow rate, temperature, yield) in case of spray drying [17, 36-38]. In emulsion-solvent evaporation, the main drawbacks are associated with low yield, insufficient encapsulation efficiency of drugs and protection of drugs in the harsh environment (stomach) and inefficient release of drugs in the targeted site [17, 25-29]. Since the microemulsion and microspheres have been prepared in a single step, drugs are exposed to harsh

organic solvents, mechanical agitation, water-oil interface, hydrophobic interaction with polymer matrix resulting in drug denaturation [16, 25, 39-43].

1.3.3. Novel targeted intestinal drug delivery system: A systematic approach

It is clear that one of the major technical challenges of developing oral drug/vaccine is mainly associated with the destabilization of biopharmaceuticals in acidic environment of stomach (pH = 1-3). There are various commercially available pH-sensitive polymers which can be used for targeted delivery. However, these cannot be easily tailored to develop target-specific drug/vaccine delivery. To this end, we synthesized pH-responsive poly (methyl methacrylate-co-methacrylic acid) copolymers using free radical solvent polymerization which was used to develop MPs for target specific sites of the small intestine as shown in the Figure 1.2. The prepared polymers were characterized by proton NMR, GPC, FTIR and pKa acid-base titration. Further, the copolymers were employed to fabricate MPs with pH-responsive macropores by O/W emulsion/solvent technique reported by Kumar et al. in our group in the development of intestine-targeted drug delivery systems [16,25,102].

After sonication-Synthesis of MPs with pores	Encapsulated samples after Freeze drying	pH 2.0	pH 7.1
		Simulated gastric fluid 2 hours at 37 °C	Simulated gastric fluid 2 hours at 37 °C
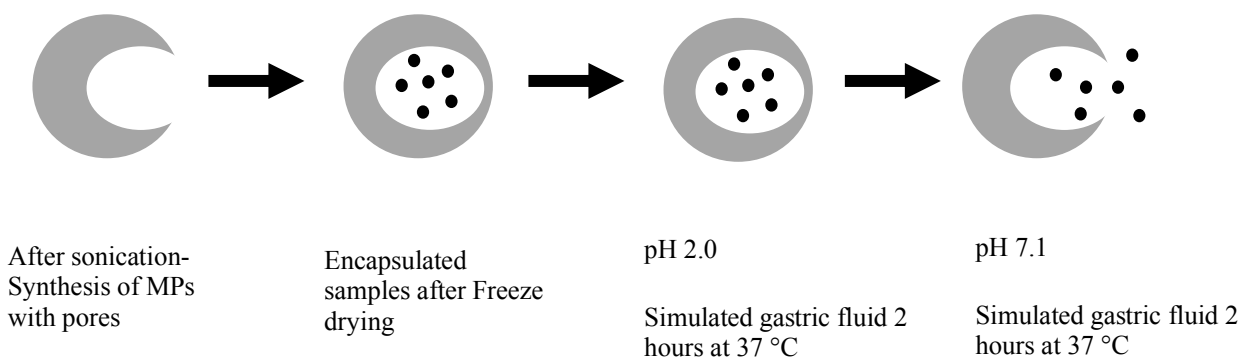
Figure 1.2. Schematics of the novel delivery system mechanism of delivery by triggered environmental conditions in the GI tract.

6

The encapsulation was carried out and pores were closed by custom-designed freeze-drying process [25]. The fabrication of MPs and encapsulation of drugs/vaccine occur through independent processes, resolving the above-mentioned destabilization and denaturation of drugs [16,25]. The pH-responding release behaviour of the pored MPs was examined by monitoring time-dependent release profile of encapsulated 100-nm fluorescent nanoparticles in simulated GI tract environment. We also encapsulated β-Galactosidase from aspergillus Oryzae for stability studies in acidic environments. Our pH-sensing polymer and MPs will advance the current microencapsulation technology by solving key challenges in encapsulation, protection, and release of oral drugs and biopharmaceuticals.

1.4. Transdermal drug/vaccine delivery

Transdermal drug delivery system is an alternate way to administer drugs to minimize and avoid the limitations caused by oral and other drug delivery systems [61]. Steady-state drug levels, drug denaturation due to GI tract effects, easy administration is some of the advantages over other drug delivery routes [62-65]. Transdermal patches are user-friendly, i.e. it can be self-administered, and has very less pain sensation compared to hypodermic injections [66].

Skin is a multilayered organ consisting of two tissue layers epidermis and dermis [68]. Epidermis comprises of keratinocyte which composes of 95% of the cells making it the principle cell along with melanocytes and Langerhans cells [69]. The second layer of skin comprises of collagen and elastic fibers, the dermis [61]. Transdermal delivery avoids deeper penetration which avoids activation of nerves to send pain signals as compared to intramuscular and intravenous injections [70]. Although it has so many advantages over other drug delivery systems, it also has certain barriers such as limited penetration through the skin caused by stratum corneum (SC), the

outermost layer of skin [67] and also human skin which has very poor permeability – as most of the drugs do not enter the skin at therapeutically relevant rates [71]. Chemical enhancers can increase the permeability of skin to small molecules but are dangerous as they can cause irritation [64]. Despite skin irritation, iontophoresis is used to deliver some peptides and small proteins [71]. Later, electroporation [72] and ultrasound [73] methods have been deployed to delivery both macromolecules and small drugs. However, more efficient work is being done to increase the drug stability, viability and efficiency of drug absorption using these methods as it cannot be used for delivery of vaccines [72]. The first ever transdermal delivery of drugs was developed to treat motion sickness which delivers scopolamine drug using patches in the year 1979 in the United states [74]. Further, there has been tremendous research conducted, and today there are several transdermal delivery systems available commercially [74, 13].

Microneedles fabricated by microfabrication methods are cost-effective strategy to deliver vaccines to humans/animals [75, 89, 94]. Hence, microneedles have been developing as effective carriers for delivery of macromolecules and vaccines such as influenza, insulin and parathyroid hormones as they maintain the stability of biopharmaceuticals and protect the vaccines from unfavourable conditions. These microneedles however must be fabricated by materials that could meet all those requirements along with biocompatibility or biodegradability.

1.4.1. Microneedles as an effective transdermal drug delivery system

The microneedle system generally may consist of an array of needles ranging from 10 to 100 microns in length and 10-400 microns in base diameter allowing them to create micron sized channels through skin without causing any pain and also allowing large molecules to penetrate through SC and reach the blood stream [76, 80]. Due to short length, microneedles require less

mechanical strength to achieve skin penetration and subsequent drug delivery. Sebastien et al in their study [71], have developed transdermal approach for humans using microneedles. They have designed a drug delivery system that enhances the transport of molecules across skin [77-79]. They have used standard microfabrication techniques to create silicon microneedles. When these silicon microneedles were inserted into the skin, they create conduits for transport across the stratum corneum (outer layer of skin – primary barrier of transport). Once, this was achieved, they could diffuse rapidly and get absorbed by capillaries for systemic administration [71, 76]. The use of microneedles is an invasive drug delivery method wherein an array of needles which are of micrometer size penetrates skin without stimulating the proprioceptive nerves [81]. However, animals in general have tougher skin which means that a higher mechanical force would be required for successful penetration. Reports have suggested that the world consumes more than four times the quantity of meat than fifty years ago [82], where the average person in the world consumes roughly 43 kilograms of meat as in 2014, pig meat being the most popular meat globally [82].

Animals are exposed to diseases more likely similar to humans which can be prevented by vaccines [83]. For example, Rinderpest, a lethal disease that killed nearly every cow it infected and was completely eradicated by 2011 by the use of vaccines [83,84]. Vaccinating animals not only protects animals from diseases but also protects humans who consume meat form transmittable diseases [85]. Influenza A primary IAv-s of strains H1N1 and H3N2 are the major strains infecting the respiratory tract in most mammals [86]. Infections can generally occur through nose-to-nose contact between different pigs, as well as between pigs and humans [87], while vaccination continues to be the best means of prevention [88]. Though IAv-s are of zoonotic importance but not primarily a food safety concern, the biggest fear of public health is the rearrangement of IAv-s into

novel strain infecting human population as in the case of influenza pandemic in 2009 [86]. Similar to influenza, there are many other viruses such as porcine circovirus type 2, porcine reproductive and respiratory syndrome, cysticerci, trichinella spiralis which clearly infects humans and is a major food safety concern [86]. To this end, we hypothesized that by synthesizing biocompatible, environmental protective stronger microneedles, we not only use them to deliver vaccines to humans, but also can be delivered to animals which could evade any transmittable diseases. Polymeric microneedles, hollow microneedles made of metals, sugar-based needles have been discovered for several decades to improve drug loading, encapsulation efficiency, preservation of drugs/vaccines, increased mechanical strengths and to deliver them successfully across the skin [90, 98].

1.4.2. Microneedles for vaccine delivery: An attempt to increase mechanical strength and environmental stability

In this work we have used milling technique using rapidly spinning microscale drills bits to physically remove materials from the substrate to manufacture 10×10 aluminum master with the needles of 400 micrometer in length. Micromolding technique was used to fabricate the negative mold of aluminum master using PDMS, and further to prepare PLA molds which had the sample replica of the aluminum master using micromolding technique. We further prepared various second generation PDMS molds which were employed to synthesize the drug-loaded final sugar-based polymer coated microneedles. To further increase the mechanical strength of microneedles we fabricated cellulose nanocrystal (CNC) microneedles using microfabrication and micromolding techniques. Microneedles with different amounts of CNC in the formulation were fabricated to investigate their effects on mechanical strength. Further we built a custom designed

spray coating device with fine nozzle to uniformly coat the microneedles with pH sensitive, Eudragit S 100 to improve the storage stability and protect the microneedles from the environment. Our CNC microneedles will advance the current sugar-based microneedles with higher mechanical strength and greater drug stability and would be the future way of delivering vaccines over conventional needle injections.

1.5.   Hypothesis and research objectives

Considering the technical challenges of the commercially available polymers and delivery systems, this research will be focused on the synthesis of anionic copolymers with different acid dissociation constant values by varying hydrophobic/hydrophilic ratios in the copolymer. These copolymers can be used as a key component to fabricate MPs with a pH-responsive macropore, following the procedure developed in our group, and microneedles with improved mechanical/environmental stability. Also, efforts need to be directed toward development and evaluation of encapsulation techniques/formulations which are compatible with the sensitive nature of biopharmaceuticals. The new formulations based on MPs and microneedles can also provide a platform for the development of universal oral and transdermal drug/vaccine formulations, respectively, with high efficacy and long-term stability. Drug/vaccine formulations can be also modified to meet i) oral administration-specific requirements for delivering drug/vaccine efficiently, i.e. protection against acidic pH of stomach, efficient release in the intestine, and   ii)   transdermal   administration-specific   requirement   such   as mechanical/environmental stability. The detailed plan to overcome these challenges is illustrated below.

For the first part of the work, our efforts will be dedicated to the following:

1. Synthesize various copolymers of poly (methyl methacrylate-co-methacrylic acid) with different acid dissociation constants.

2. Fabricate microparticles with pH-responsive macropores

3. Successful pore closure by lyophilisation process after encapsulation of ingredients

4. Examine the pH responsiveness of the microparticles by conducting release tests of model and real drugs in simulated digestive conditions

Further for the next research goal, our efforts will be dedicated to the implementation of CNC as a viscosity enhancer into formulations for fabricating microneedles:

1. Micromilling aluminum master molds with a conical microneedle design (length: 400 ± 20 µm, base diameter: 300 ± 15 µm)

2. Use micromolding techniques to fabricate PDMS, PLA and CNC microneedles

3. Study the effects of the amounts of CNC in the formulation and the formation of a protective coating on the mechanical strength of microneedles

4. Pig skin insertion test of the developed CNC microneedles

2. Materials and methods

2.1. Materials

Tetrahydrofuran (99% HPLC grade), 2-propanol (ACS reagent), and Tween-20 were purchased from Fisher Scientific. 2-Nitrophenyl B-D-galactopyranoside from Aspergillus Oryzae, galactose and lactose assay kit, disodium hydrogen phosphate, methacrylic acid (MAA), methyl methacrylate (MMA), 2,2'- Azobis-(2-methyl-propionitrl) (98%), inhibitor remover, Polyvinyl alcohol (PVA) M_w: 9,000-10,000 Da, bovine serum albumin, ethanol (ACS reagent), and acetone (ACS reagent) were acquired from Sigma-Aldrich (St Louis, Missouri, USA). Yellow-green fluorescent nanoparticles (100 nm) were purchased from Life Technologies (Thermo Fisher Scientific, Waltham, MA). Aluminum microneedle master was fabricated using a micromilling workstation (Model number 363-S; Microlution Inc, Chicago, IL, USA). SYLGARD™ 184 Silicone Elastomer Kit, consisted of silicones and curing agent to be mixed in the ratio of 10:1 for making PDMS solution, was purchased from Dow chemicals. Cellulose Nano Crystals (CNC) sample was kindly donated by Alberta-Pacific Forest Industries Inc. (Edmonton, Alberta, Canada). Carboxymethyl Cellulose, sodium (low viscosity), Trehalose dihydrate (from Saccharomyces cerevisiae > 99%), Sucrose (BioUltra for molecular biology > 99.4%) HPLC grade, Dichloromethane (anhydrous, 99.7%), and polycaprolactone (M_w = 45,000/80,000 Da) were purchased from Sigma-Aldrich.

2.2. Synthesis of pH sensitive poly (MMA-co-MAA)

The co-polymer was synthesized by free radical solvent polymerisation in tetrahydrofuran. Our goal was to synthesize a library of poly (MMA-co-MAA) with different pKa values and low

13

molecular weight. This was achieved by taking different molar feed ratio of monomers (MMA: MAA), i.e. 90:10, 80:20, 70:30, 60:40 and 50:50. Inhibitors were removed from both monomers by passing them through a column filled with inhibitor remover (Cat. No.: 306312, Sigma-Aldrich). The experimental setup is shown in the Figure 2.1. Required quantity of the solvent (i.e., tetrahydrofuran) was taken into a three-necked round-bottom flask immersed in the oil bath placed on the hot stirrer plate. The monomers were added in succession to the solvent using glass pipettes.
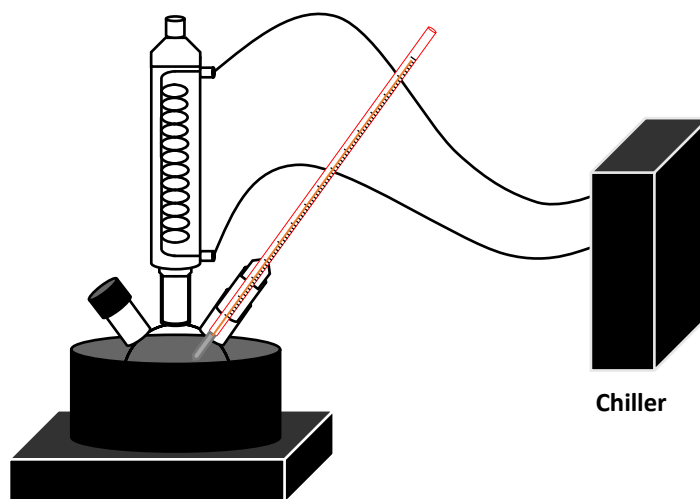
Figure 2.1. The experimental setup used for the free radical solvent polymerisation at 70 °C. The reaction was conducted under inert nitrogen atmosphere.

The mixture was stirred homogeneously using a magnetic stirrer at 150 rpm. 2,2'- Azobis-(2-methyl-propionitrl) (98%) (AIBN) initiator (1.5 wt% of comonomer concentration) was weighed and mixed with the contents in the flask. One of the necks was closed using a rubber cork and sealed using thick copper wire. A condenser was fitted to the other neck of the flask, which was connected to a circulating coolant. The cooler was set to -15 °C for efficient heat transfer to condense the vapors of the low-boiling point solvent. A thermometer was installed in the third neck to regulate and maintain the temperature inside the reactor. Since the initiator decomposition

temperature (k_d) is reported to be > 65 °C [17], condenser was used to condense the vapors of the solvent (boiling point: 60 °C). After the setup, the mixture was stirred to completely dissolve AIBN. It is noted that all the components in the reactor are readily miscible with each other. One of the inhibitors on the propagation mechanism of free radical copolymerisation is the presence of oxygen, thereby the mixture was bubbled with N_2 gas for an hour and the reaction was subsequently carried out under nitrogen atmosphere.

After bubbling, the temperature was subsequently increased to 70 °C to initiate the polymerisation. The reaction mixture became turbid, followed by the formation of a thick and viscous liquid, indicating the formation of the polymers. After 4 hours, methanol was added to quench/inhibit the polymerisation. After the solution was cooled down to room temperature, the polymer was precipitated in deionized (DI) water, and reprecipitated in acetone to remove methyl methacrylate monomer and poly (methyl methacrylate) homopolymer. The product was further washed (i.e., reprecipitated) with DI water to remove unreacted methacrylic acid monomer and poly (methacrylic acid) homopolymers [55]. The copolymer was dried and stored in an incubator at 60 °C. The first batch of copolymers of feed molar ratio 66:33 and next batch 75:25 of MMA: MAA were synthesized using the similar conditions, and the copolymer characteristics such as molecular weight, copolymer composition and functional group analysis were performed. Further, batches of copolymers with different pKa values were synthesized.

2.2.1. Thermogravimetric analysis

The weight of the purified polymer stored in the incubator at 60 °C was recorded periodically until it remained constant. The weight of the initiator was subtracted from the total

weight in order to calculate the amount of polymeric material produced at a given time. The conversion is calculated by

$$Converstion = \frac{Initial\ weght\ of\ monomers - Final\ dry\ weight\ of\ polymer}{Initial\ weight\ of\ monomers}$$

2.2.2. Fourier-Transform Infrared spectroscopy (FTIR)

FTIR spectroscopy (FTS 7000 Series by DIGILAB) in the range of 4000-400 cm^{-1} was employed to determine the functional groups present in the copolymer and to compare the compositions of the copolymers.

2.2.3. Gel Permeation Chromatography (GPC)/ Size Exclusion Chromatography (SEC)

The molecular weights of the synthesized copolymers were determined using high temperature GPC (Malvern, VISCOTEK HTGPC) in HPLC grade tetrahydrofuran (20 mg/mL). The calibration of GPC column was performed using polystyrene standards (Peak molecular weight, M_p = 1000, 3000, 5000, 7000, 10000, 20000, 30000, 50000, 100000 g/mol).

2.2.4. ^{1}H Nuclear Magnetic Resonance spectroscopy

The ^{1}H NMR spectroscopy was recorded using 500 MHz Bruker spectrometer within the Canadian National High Field NMR Centre (NANUC) at the University of Alberta. Copolymers were dissolved in DMSO-d$_6$ solvent at a concentration of 60 mg/mL for NMR analysis. NMR was performed to quantitatively characterize the copolymer composition. Due to difference in the reactivity of monomers (i.e., MMA and MAA), the composition (mol %) taken in the feed will not be same in the copolymer composition [49,56]. This is due to the composition drift occurring during

the polymerisation process. To this end, the reaction can be done in a semi-batch reactor (variable flow of one monomer so that the ratios of the monomers present in the reactor remains same throughout the reaction) or may be terminating the reaction at lower conversion [49].

2.2.5. pKa measurement by acid-base titration

To determine pKa values (acid dissociation constant), acid-base titration was carried out. Copolymers were dissolved in 0.1 M NaOH solution (0.5 mg/mL), which was titrated against 0.05 M HCl solution. Also, different pH solutions (pH 4.0 to 8.0 with 0.1 increment steps) were prepared using pH meter (HI 2213 pH/ORP meter; HANNA instruments, Woonsocket, RI, USA) with the use of NaOH and HCl solutions in DI water.

2.3. Fabrication of MPs with macropores

MPs were fabricated using oil-in-water (O/W) emulsion followed by a solvent evaporation as shown in Figure 2.2. previously reported by Ankit et al [25]. The organic phase was prepared by dissolving 5 wt% of copolymers dissolved in cosolvent system (dichloromethane: ethanol: isopropanol = 2:1:1). The aqueous solution was prepared by dissolving 0.5% (w/v) of polyvinyl alcohol and 5% (v/v) of Tween 20 in DI water. Briefly, 200 mL of aqueous solution was taken in a beaker and the tip of the sonicator (GE-130 Ultrasonic Processor; Sonics and Materials, Inc, Newtown, CT, USA) was immersed into it. 10 mL of organic phase was added to the aqueous phase using a pipette immediately after sonication (30 % amplitude) while stirring at 325 rpm. After sonication for 5 min, the solution was transferred to one litre beaker and stirred for an hour for solvent evaporation.

2.3.1. Purification and pore closure of MPs

The prepared MPs were filtered using a mesh strainer (45 Fisher brand TM 4552 brass, 325 Mesh, 45 µm sieves), followed by centrifuge-washing with DI water (Eppendorf model 5810/5804 R) multiple times to remove the surfactant completely. Furthermore, the trace amounts of solvents were removed using rotary evaporator at 50 °C for 10-20 min (Büchi R200; Labortechnik), followed by washing with DI water. The MP samples were freeze-dried by using the previously reported lyophilisation process [16,25]. Briefly, the concentrated MPs were transferred into 2 mL Eppendorf tubes, which were then frozen in liquid nitrogen and transferred to freeze-dryer (AdVantage Pro Freeze-dryer; SP Scientific, Warminster, PA, USA). MP samples were stored at 4 °C until further use.

2.4. Encapsulation of fluorescent nanoparticles (100 nm- model drug)

100 nm FNPs mimicking the size of vaccines were used as model drugs. The fluorescent nanoparticles 2 wt% solids were diluted 10-fold in the formulation (15% (w/w) trehalose + 0.5% (w/w) low viscosity carboxymethyl cellulose (CMC) in DI water) prior to encapsulation experiments. 1 mL of the 10-fold diluted fluospheres (FNPs) solution was added to 30 mg of MPs, followed by repeated vacuum cycles for encapsulation of fluospheres [25]. After encapsulation, the FNP-encapsulated MPs were separated from unencapsulated FNP suspension by centrifuge at 500 rcf for 2 min, followed by resuspension in 1 mL of the trehalose + CMC formulation. Samples were then freeze-dried to seal pores.

2.4.1. Release test of FNP-encapsulated MPs

The freeze-dried FNP-encapsulated MPs were incubated in simulated gastric fluid (SGF- 0.05 M KCl and 0.05 M HCl added to make pH 2.0) for 2 hours at 37 °C and in simulated intestinal fluid (SIF- consisting of KCl (0.05 M), HCl (0.05 M) and saturated Na_2HPO_4 added to make pH 7.1) for 4 hours at 37 °C. A time-dependent release of FNPs from MPs in the GI tract was analysed by measuring the fluorescence intensities by SPECTRA MAX GEMINI XS (Molecular Devices; San Jose, CA, USA) at different time intervals when subjected to GI tract environments. Further, the pH-dependent release behavior of FNPs was monitored using the fluorescence microscope (AmScope, Irvine, CA, USA) over time.

2.5. Encapsulation and release test of lactase-encapsulated MPs

200 mg of β- Galactosidase from aspergillus (Lactase) was dissolved in 10 mL formulation (15% (w/w) trehalose, 0.5% (w/w) low viscosity CMC in DI water). 1 mL of the solution was added to 30 mg of MPs. The lactase was encapsulated into the pored MPs following a similar procedure to FNPs. MP pores were then closed by freeze-drying process as described in 2.3.1.

2.5.1. Biological Assays

The protein concentration and the remaining activity of the enzyme were measured by micro BCA assay and ONPG assays, respectively. The control has polymer MPs freeze-dried in the trehalose + CMC formulation which was dissolved in SIF containing all the moieties present in the lactase-encapsulated MP sample.

2.5.1.1.   Micro BCA assay to determine the protein concentration

Micro BCA assay is used to determine the protein concentration that has been encapsulated into MPs. 20 mg/mL BSA (Bovine Serum Albumin) was prepared in DI water and BCA assay reagents were prepared following the standard protocol mentioned in the protein assay kit (Pierce BCA Protein Assay Kit; Thermo Fisher Scientific, Waltham, MA, USA). The three rows of standard were prepared starting from BSA concentration starting from 200 µg/mL. Two times serial dilution with polymer background were performed and the last column had zero BSA concentration. At the end, the series of the concentrations in standard wells were 200, 100, 50, 25, 12.5, 6.25, 3.125, 1.56, 0.78, 0.39, 0.195, and 0 (µg/mL). 150 µL of the lactase encapsulated MPs sample was taken in at least 5 wells. If the sample seemed to be concentrated, it was diluted and then 150 µL of the BCA working buffer was added to every background as well as the sample. The plates were further incubated at 37 °C for 60 min and absorbance was measured at 562 nm wavelength by i-Mark microplate reader (Bio-Rad Laboratories, Inc., Hercules, CA, USA).

2.5.1.2.   ONPG assay to determine the remaining activity of the drug

For ONPG assay, 20 mg/mL lactase (β-Galactosidase from Aspergillus Oryzae) and 4 mM ONPG (ortho-nitrophenyl-β-galactosidase) were separately prepared in DI water under magnetic stirring. Three standard rows of lactase of known concentration diluted with polymer background were prepared starting from lactase concentration of 200 µg/mL. Serial two-fold dilutions were done as the concentrations in standard wells were 200, 100, 50, 25, 12.5, 6.25, 3.125, 1.56, 0.78, 0.39, 0.195, and 0 (µg/mL). 50 µL of the lactase-encapsulated polymer sample was added to at

least 5 wells. 100 μL of ONPG solution was added to all the wells, followed by incubation at 37 °C for about 60 min prior to absorbance reading at $\lambda = 410$ nm.

2.6. Micromilling
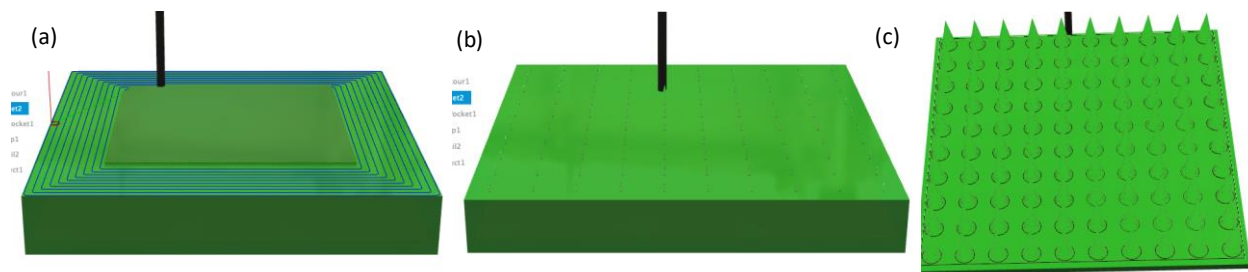
Figure 2.2. Images of model progression of micro-needle simulation from 1×1 cm² block at the initial (a), intermediate (b), and (c) final stages of micromilling

The experiments for fabricating the aluminum master molds were conducted by Dr. Surjith Kumaran (Research Associate) and Mr. Matthew Lawson (Graduate student) in our group. The micro-milling experiments were carried out by using a Microlution 363 S CNC milling machine. To fabricate conical cone-shaped solid microneedles, tight-tolerance 6061 Aluminum (Mc master Carr) was used, which was cut into 1"×1"×0.25" (W × L × T) mounted on a pallet. The design, simulation (Figure 2.2) and G-code generation of sharp tip microneedles were conducted using Fusion 360 (Autodesk). The G-code was inputted into CNC control platform, a machine controller PMAC2 and then a motion program, which drives the machine axes. Solid carbide end mill (1/8″ diameter, 150 micro tip diameters purchased from Performance micro tools Inc.; Janesville, WI, USA) were used for machining a microneedle base and microneedles as shown in the Figure 2.2.

For modeling of the microneedles, 350 cm diameter circles were first drawn and then, 10×10 circles are placed at 750 micrometers (center to center) apart. Microneedle shape was drawn using Extrude function with Z-axis distance of 1 mm and taper angle ‾10 degree. The obtained

21

model is simulated using milling 3DPocketing function of AutoCAD Fusion360. Cutting feed rate for making microneedles were set to 10 mm/min with the spindle speed of 15,000 rpm. The smoothness tolerance is opted at 0.001 mm with step 8 mm/min. After the aluminum master was made, it was cleaned and rinsed with isopropanol and ethanol. It was stored in the incubator at 60 °C until was used for the micromolding process.

2.7. Fabrication of CNC molds polydimethylsiloxane molds

Polydimethylsiloxane (PDMS) is a well-known for its viscoelastic properties and is the mostly used silicon based organic polymer due to its flexibility. The negative mold of the aluminum master was prepared using PDMS. The Sylgard 184 silicone elastomer was mixed with the hardening reagent in the ratio of 10:1 (w/w). The solution was stirred well for two minutes using a glass rod. Further, the solution was degassed for the complete mixture and removal of bubbles. After the solution was degassed, it was poured into the aluminum master filling them completely. They were subjected to multiple cycles of vacuum to remove any residual gas voids. Vacuum was applied to ensure that the highly viscous liquid fills the microstructure perfectly. The aluminum master with the liquid mixture was further kept in the incubator at 90 °C for two hours for PDMS crosslinking. Once the reaction was done, it was then demolded from the aluminum master. To avoid any damage to the aluminum master and increase the recyclability, we further fabricated a positive PLA structure similar to aluminum master and used them for further productions of second generation negative PDMS molds. PLA pellets (thermoplastic polymer) on the PDMS mold were heated up to around 200 °C. After several vacuum cycles, the molds were pressed with a stainless-steel bar at room temperature. The solidified PLA microneedle patch was demolded from the first generation PDMS mold. The process was repeated several times as to

make several second generation PDMS molds in a single batch. These PLA molds exactly mimic the aluminum master needles, and these were used to make a series of second generation PDMS molds, making it more cost-effective. The fabricated second-generation PDMS molds were used for making CNC microneedles. The schematics are shown in Figure 2.3.

2.8. Formulations used for fabrication of CNC microneedles

Formulations play an important role in maintaining the stability of the biopharmaceuticals. In the past sugar-based CMC microneedle formulation have been used as it maintains the stability of the biopharmaceuticals, however these needles didn't have mechanical strengths to penetrate animal's skin [97, 99, 100]. We prepared different concentrations of Cellulose Nano Crystals (CNC) ranging from 0.01% (w/w), 0.1% (w/w), 0.25% (w/w), 0.5% (w/w), 0.75% (w/w), 1% (w/w) and 2.5% (w/w) + 15% (w/w) trehalose in DI water (hereafter abbreviated as CNC formulation). We also prepared 0.5% (w/w) CMC + 15% (w/w) trehalose solution in DI water (hereafter abbreviated as CMC formulation) as a sugar-based microneedle for control. Further the stability of vaccines is
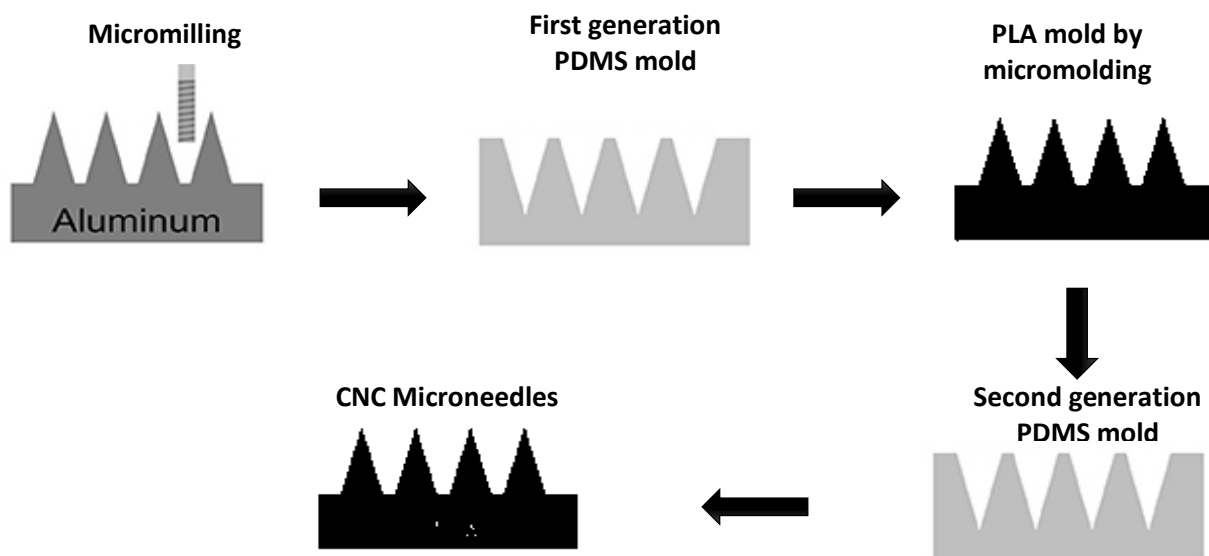
Figure 2.3. Fabrication of CNC microneedles from aluminum master by micromolding process

dependent on the viscosity enhancer of the sugar-based formulations. Therefore, we prepared different concentration of CNC formulations and measured the viscosity using rheometer (HR 2; TA instruments, New castle, DE, USA). These formulations are then stored at 4 °C. Model drugs (i.e., 100nm sized FNPs) were diluted to 0.02 wt% solids using the above-mentioned formulations for encapsulation purposes. CMC backing is required for the successful demolding of the needles form PDMS molds. Thus, we prepared a formulation consisting of 15% (w/w) CMC (low viscosity) + 10% (w/w) trehalose in DI water (hereafter abbreviated as CMC backing formulation). The formulation was then degassed to remove bubbles and stored in incubator at 37 °C before use. To investigate the effects of anionic copolymer coating on the surface of microneedles, we also prepared microneedles coated with pH sensitive Eudragit anionic S100 obtained from Evonik industries (Burlington, Ontario, Canada). For the polymer coating, 2 g of S100 (M_w: 125,000 g/mol) was dissolved in 40 mL of co-solvent consisting of dichloromethane, ethanol and isopropanol in the ratio of 2:1:1, respectively (hereafter abbreviated as polymer formulation).

2.9. Encapsulation of FNPs and fabrication of CNC microneedles

150-200 µL of CNC formulation mixed with ingredients was pipetted on to the PDMS mold. 100 nm FNPs mimicking the size of influenza vaccine was mixed with CNC formulation. It was then vacuumed several times to remove bubbles and gas voids from the PDMS molds for successful encapsulation. After the vacuum encapsulation process, the excess formulation

Figure 2.4. (a) Showing the encapsulation of CNC formulation with dye/drug after vacuum. (b) showing the encapsulation of CNC formulation with dye/drug after centrifugation

remaining on the molds was removed using a pipette. The molds were centrifuged at 3000 rpm for

5 minutes. After centrifugation, the molds were cleaned using Q-tips to completely remove any

further unencapsulated ingredients. These molds are kept in the incubator at 37 °C for 4 hours for

drying the CNC needle formulation. The sugar-based needles were also prepared using similar

methods. The Figure 2.4 shows the difference before and after the centrifugation process. After 4

hours of drying, the molds were taken out form the incubator. CMC formulation was

spread/applied over the mold using a spatula. The mold was subjected to vacuum to remove

bubbles and to ensure the CMC backing completely filled the mold. The molds were removed

from the vacuum oven and the sides were cleaned using Q-tips.
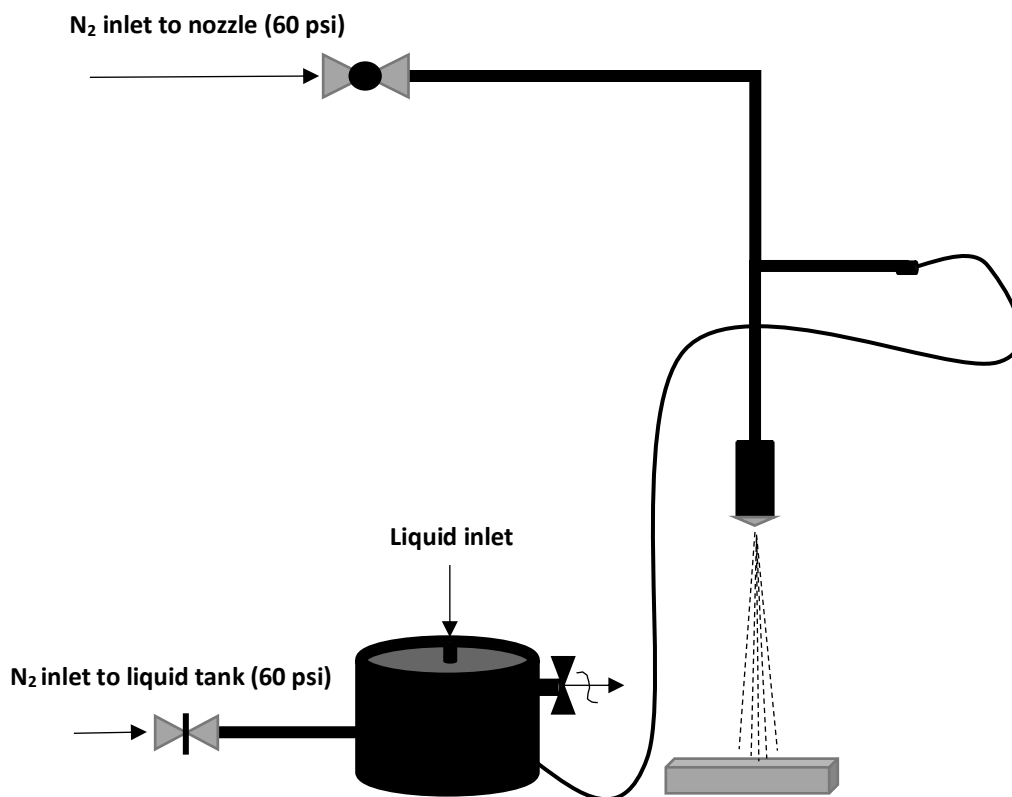
Figure 2.5. The schematics of the customed designed spray coating system by our group. Nozzle was purchased from Spraying Systems Canada; fittings were purchased from Swagelok (pharmaceutical grade stainless steel)

Further it was stored in the incubator at 37 °C for 12 hours. Finally, the CNC microneedles are demolded from the second generation PDMS molds. the skin. Further, we came up with an efficient way to coat the needles with polymers by spray coating as shown in the Figure 2.5. The spray coating machine was used to form a polymer protection coating on the CNC microneedles. For this purpose, we have custom-designed an atomized spray coating device (see Fig. 2.5 for schematic of the spray coating system). Spray coating was employed to get a uniform layer of coating of desired thickness by controlling the distance of the sample from the nozzle and exposure time. The needles were placed of about 22 cm below the nozzle. The co-solvent solution was first used to rinse the system. After rinsing, 5 wt% Eudragit S100 (Evonik, Germany) polymer solution was loaded into the pressure vessel. Nitrogen gas was used to pressurize the liquid polymer solution (60-80 psi). There was a separate gas valve inlet to the nozzle along with the liquid inlet to atomize the spraying with fine particles. First the liquid valve was opened, following the opening of the gas valve inlet atomizing the spray coming off the nozzle.

2.10. Imaging

Scanning Electron microscopy (S-3000N; Hitachi, Chiyoda, Tokyo, Japan) was used to analyse the morphology and surface pores of the MPs. Fluorescence microscopy (AmScope, Irvine, CA, USA) was used to image the time dependent release of FNPs from MPs. The structure of the microneedles was observed and imaged by optical microscopy (Cole-Parmer, Vernon Hills, IL, USA), fluorescence microscopy and scanning electron microscopy. Moticam digital microscope camera was used to capture images of the needles through the microscopes. SEM was used to analyse the detailed surface morphology of PDMS mold, and microneedles before and after coating with Eudragit S100. Since MPs and microneedles were not electrically conductive,

26

they were coated with 10-20 nm Au/Pd layer and analyzed at 10 kV and 5 µA at a working distance of 8 mm to 15 mm.

2.11. Mechanical properties of microneedles

Force

Test structure: 400 µm
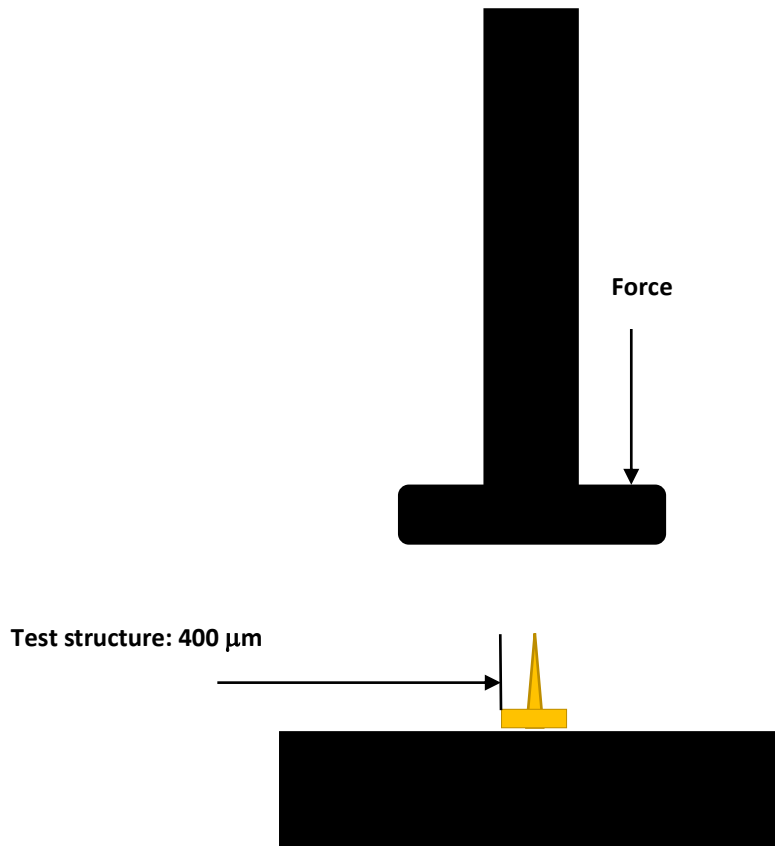
Figure 2.6. Schematics for the mechanism of measuring the failure force of microneedles

The failure force of the microneedles was investigated by measuring the axial force required to break or bend the microneedles using a rheometer (Discovery HR 2 series; TA instruments, New Castle, DE, USA). The effects of both CNC concentration and S100 protection layer on the mechanical properties of microneedles were analysed from the force vs. displacement curves generated using a rheometer. As shown in Figure 2.6, the 10×10 microneedle patch is placed on the lower bottom surface with the needles facing upwards. This set-up was used to apply

27

a normal load on the microneedles with a constant velocity of 2 μm/s. The obtained force vs. displacement graph was used to predict the force necessary for breaking the microneedles [104,105].

2.12. Skin penetration test using CNC microneedles

Pig's skin is rigid and hard compared to human skin making it difficult to insert microneedles through the skin. One interesting idea was to deliver the vaccine through microneedles to pig ears, which could be manageable. Hence, the isolated pig skin was washed and cleaned using isopropanol. The CNC microneedles were held and pressed against the pig's skin for 10-15 seconds. The needles were removed, and the tissues were stained with tissue marking dye (Fisher Scientific). They were further cleaned using isopropanol and viewed under optical microscope.

3. Results and discussion (Microparticles)

3.1. Synthesis and characterization of poly (MMA-co-MAA) copolymers

Random poly (MMA-co-MAA) copolymers with different molar MMA: MAA ratios (i.e., 90:10, 80:20, 70:30, 60:40, 50:50, and 100:0) were synthesized by free radical polymerisation with the appropriate mixture of monomers, initiator and solvent. The properties of the produced copolymers were characterised by FTIR, GPC, NMR, thermogravimetric analysis, and pKa titration.
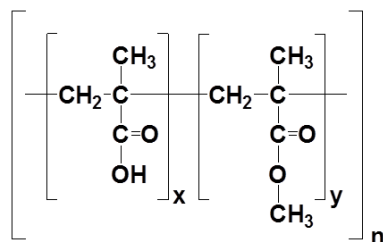
Figure 3.1. The structure of the pH sensitive copolymer poly (MMA-co-MAA)

3.1.1. Conversion

Thermogravimetric analysis was performed to calculate conversion of monomers with different reactivity ratio to copolymers. Supposedly, if the reactivity of MMA is too higher than that of MAA, MMA monomers would be consumed faster than MAA monomers, resulting in the formation of gradient copolymers. This would lead to compositional drift in the final copolymer composition. To avoid the compositional drift, several methods have been proposed: 1) a constant flow of one of the monomers (semi-batch reactor) while maintain the ratios of monomers in the

reactor constant [49] and 2) low conversion polymerisation reaction. In this work, we tried to synthesize polymers with low conversion method to minimize compositional drift.

As summarized in Table 3.1, it was found that the two different batch copolymers (Serial number 1 and 2) exhibited a nearly complete conversion by thermogravimetry analysis. To avoid compositional drift, the polymerisation time was reduced from 8 hours to 4 hours. With different molar ratios of monomers, conversions of different polymerisation batches were found to be in the range of 50% to 60%. It was clear that with the decrease in polymerisation time, the conversion

Table 3.1. The monomer conversion values obtained from the copolymerisation of Methyl Methacrylate (MMA) and Methacrylic acid (MAA) monomers by free radical solvent copolymerisation.

was subsequently decreased. We expect these low conversion polymers to have lower compositional drift than the copolymers with complete conversion of monomers [49].

Serial number	Batch	MMA: MMA (feed) mol ratio	Time (h)	Conversion
1	HC 10	66:33	8	96.7%
2	HC 11	75:25	8	95.2%
3	HC 12	100:0	8	94%
4	HC 13	90:10	4	58%
5	HC 14	80:20	4	55.4%
6	HC 15	70:30	4	57%
7	HC 16	60:40	4	54%
8	HC 17	50:50	4	53.5%

3.1.2. Fourier-Transform Infrared spectroscopy to determine functional groups

Figure 3.2(a) shows FTIR spectra monitored from the products (batch HC 13 to 17 in Table 3.1) produced with different monomer ratios. The broad absorption band in the copolymer at 1705 cm^{-1} is associated with C=O vibrations of the carboxylic acid groups, and peaks at 1730 cm^{-1}, 1150 cm^{-1} to 1160 cm^{-1}, 1190 cm^{-1} to 1195 cm^{-1} and 1250 cm^{-1} to 1275 cm^{-1} indicate the further ester

vibrations [50]. However, since these functional groups are common to both monomers, they cannot be used as an indicator of successful polymerization reaction (compare Figure 3.2(a) with (b)). Also, the -OH peaks present in the range from 2500 cm^{-1} to 3500 cm^{-1} due to the hydroxyl group stretching can be accounted by methacrylic acid groups of the copolymer [50]. The broad range was also contributed by CH$_x$ present in the polymer backbone. Furthermore, from the analysis of FTIR spectra obtained from HC 13 to HC 17, it is evident that the intensity of peaks observed in the 3500 cm^{-1} and 2500 cm^{-1} range increased with an increase in the concentration of methacrylic acid in the copolymer, indicating the formation of copolymers with different compositions. When compared to the FTIR peaks of pure PMMA homopolymer where in there was only a small peak in the range between 2500 cm^{-1} to 3500 cm^{-1} generated from the -CH$_x$ groups in the polymer backbone, the synthesis of copolymers was evident. In spite of difficulty of predicting quantitative information, FTIR analysis proves the successful synthesis of poly (MMA-co-MAA) copolymers with different copolymer compositions in a controlled way.
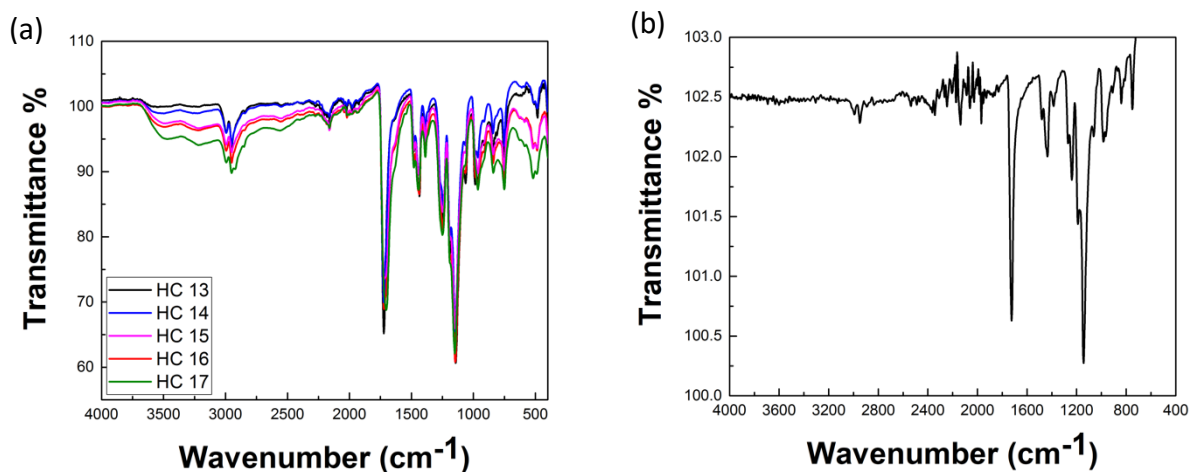
Figure 3.2. FTIR spectra of (a) copolymers synthesized by free radical polymerisation and (b) homopolymer MMA, where there isn't much of a peak formed between 2500 to 3500 cm^{-1}

3.1.3. ^{1}H Nuclear Magnetic Resonance Spectroscopy for Copolymer Compositional analysis

Due to the difference in reactivity ratios as reported in literatures [56], these monomers react at different rates, which depend on the solvent used for polymerisation, polymerisation temperature and the type of initiators. Copolymer composition was calculated by the integrated areas of the characteristic NMR peak of each monomer (see Figure 3.3 for NMR spectra and Table 3.2 for analysis summary). Considering the structural feature of the copolymer (Figure 3.1.), the unique functional groups different among the monomers are identified to be -OCH$_3$ and -OH groups. However, the peaks due to hydroxyl groups (characteristic for MAA) cannot be considered being a labile proton. It should be noted that the peak shown in Figure 3.3(a) at 12.5 ppm corresponding to hydroxyl group was not consistent with number of scans due to hydrogen bonding, which may cause huge errors in calculating the compositions of the copolymer. Instead, we could calculate the copolymer composition by investigating the peaks ranging from 1.4 to 3.8 ppm. Since -CH$_2$ /-CH$_3$ groups are present in similar ratios in each monomer in the copolymer backbone, it is reasonable to use the integrated peaks to calculate the total composition of the copolymer [51-53]. The peak at 3.6 ppm corresponds to the -OCH$_3$ peak of the methyl methacrylate present in the copolymer [51]. The peaks ranging from 0.7 ppm to 0.9 ppm and from 1.6 ppm to 2 ppm are associated with -CH$_3$ and -CH$_2$ groups, respectively, present in the copolymer [52-53]. The copolymer composition was calculated by dividing the integrated values of the -OCH$_3$ peak with integrated values of -CH$_3$ peaks (Table 3.2).
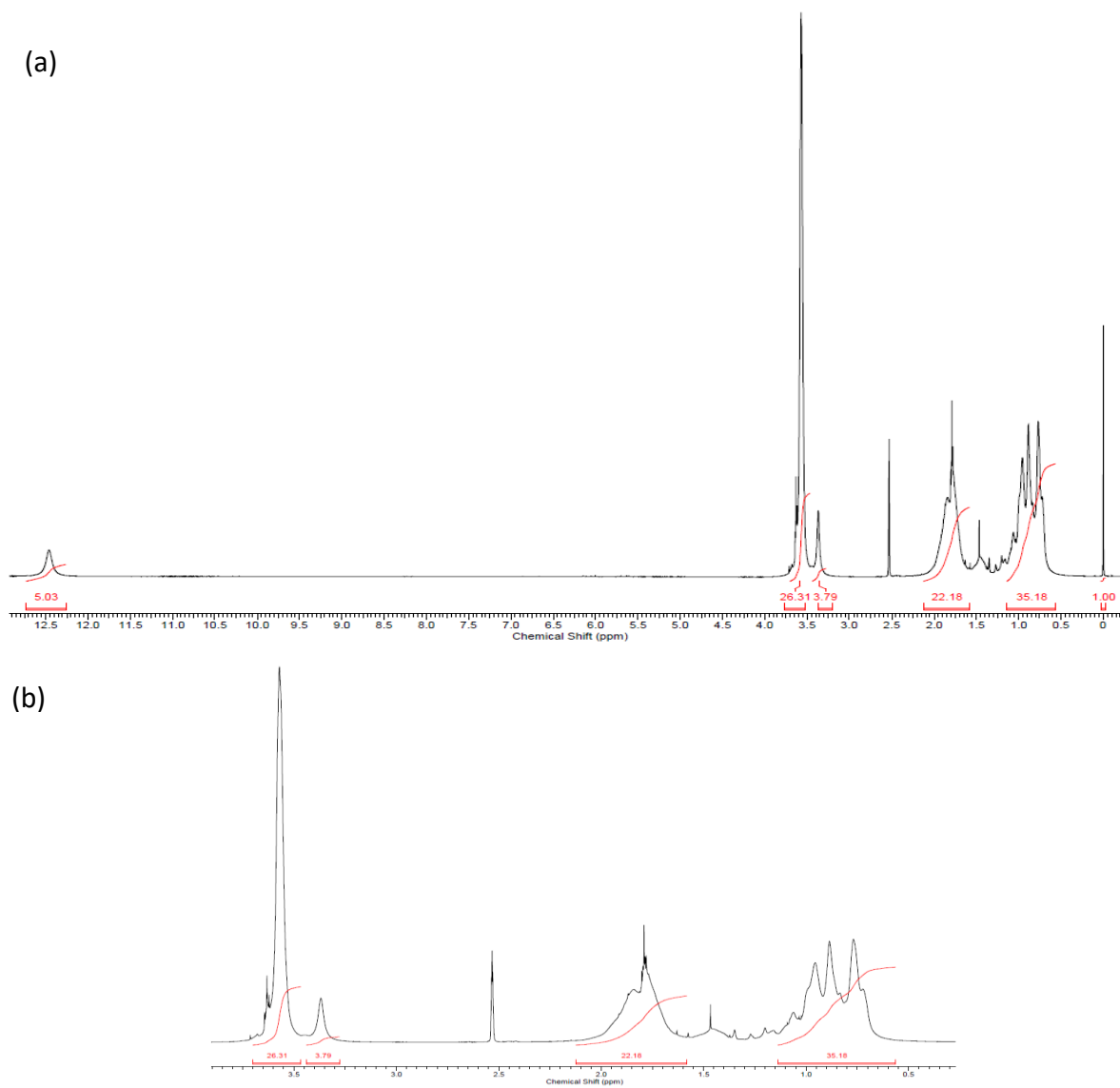
Figure 3.3. Showing the proton NMR peaks of the copolymer, the peak at 3.7 ppm being the characteristic peak of MMA group. The range of peaks were studied, and copolymer composition were analysed

Table 3.2. The copolymer composition values calculated from the integrated characteristic peaks of -OCH₃ to the total copolymer -CH₃ peaks. The values obtained agreed with the monomer feed ratios taken during the free radical polymerisation

Batch	Mol% (MMA: MAA)	Integrated - OCH₃ peaks	Integrated - CH₃ peak	Mol% MMA in copolymer
HC 12	100:0	-	-	100
HC 13	90:10	32.300	32.8214	98.4
HC 14	80:20	0.2805	0.3324	84.4
HC 15	70:30	1.1610	1.5707	73.9
HC 16	60:40	1.1167	1.7293	64.6
HC 17	50:50	0.2085	0.3606	57.8

Table 3.2. shows the compositions of copolymers synthesized with different feed ratios of monomers. It was observed that the copolymer compositions were not similar to the initial feed composition, which supports the idea of compositional drift due to variance in reactivity ratios of the monomers. From the above results, it was also found that the MMA monomers exhibited higher reactivity rates than MAA. Since, MMA has a higher reactivity ratio, the copolymer composition shifted towards increase in mol% of MMA with the increase in conversion of monomers in a batch reactor. Similar trend was observed for all the other polymerisation batches. Therefore, it is concluded that reactivity ratios of MMA to MAA must be greater than unity under similar polymerisation conditions.

3.1.4. Gel Permeation Chromatography/ Size Exclusion Chromatography for molecular weight determination

The number average molecular weight M_n, the weight average molecular weight M_w and the polydispersity index (PDI) were determined using GPC. From Table 3.3, the M_w of copolymers were measured range from 16,399 gmol⁻¹ to 21,147 gmol⁻¹. The GPC analyses gave a monomodal

distributions with the polydispersity ranging from 1.48 to 1.798 as shown in the Table 3.3. The low polydispersity can attribute to repeated precipitation of the copolymers in DI water [96]. It was studied earlier that precipitation of the polymers can result in loss of low molecular weight chains [96]. The polydispersity depends on the solvent used for polymerisation as well as the polymerisation conditions. On the other hand, the molecular weight depends mainly on the initiator to monomer ratio. With increase in initiator to monomer concentration, the molecular weight decreases. The high initiator to monomer ratio is estimated to form lots of free radicals during the initiation step contributing to chains of lesser degree of polymerisation, leading to the reduction in molecular weight of polymers formed. Hence, this means that we can synthesize polymers with different molecular weights by changing the ratios of initiator to monomer concentration.

Table 3.3. The number average and weight average molecular weights and calculated polydispersity of copolymers obtained from gel permeation chromatography for different compositional copolymers prepared by free radical solvent polymerisation.

Sample batch	M_n (gmol^{-1})	M_w (gmol^{-1})	PDI
HC 12	19,836	29,703	1.497
HC 13	6,715	12,075	1.798
HC 14	10,808	16,399	1.517
HC 15	13,730	21,147	1.537
HC 16	11,591	17,177	1.482
HC 17	10,955	16,498	1.506

3.1.5. pH responsiveness

Subsequent to the successful synthesis of the anionic copolymers, their pH responsiveness was further characterized by acid-base titration experiments (Figure 3.4). As shown in Figure 3.4(a), HC 13 exhibited two different slopes, indicating that the polymer is not responsive to ambient pH changes. Unresponsiveness to pH can be explained by the presence of small amounts of MAA units in the copolymer (i.e., ~ 1.6 mol%). As a result, HC 13 polymer did not dissolve in 0.1 M NaOH solution, a strong base with pH = 13. The other batch copolymers readily dissolved in 0.1 M NaOH solution, but similar titration curves were obtained due to very small difference in pKa values. However, the polymer solution showed a sharp change in solution turbidity when the pH decreased below their pKa due to protonation, as evidenced by the formation of cloudy precipitate with further addition of 0.05 M HCl solution (Figure 3.5). It was observed that pKa of the copolymers increased with the increase in the hydrophobic methyl methacrylate composition (Figure 3.4(b) and Table 3.4), which is consistent with a previous report [57]. The table 3.4. shows the pKa values measured by monitoring the pH before forming a cloudy solution from different batches.

(a)

(b)
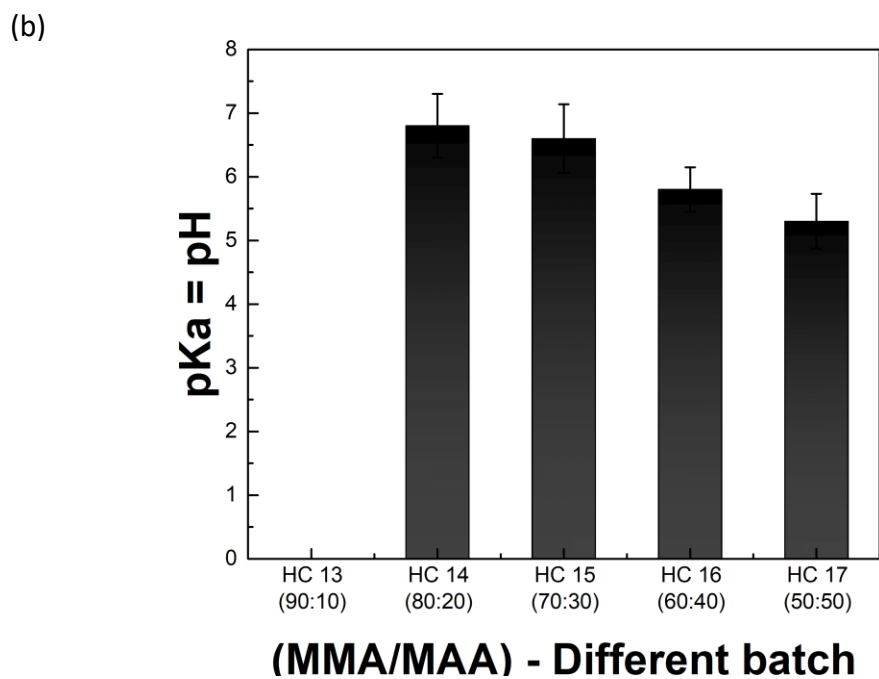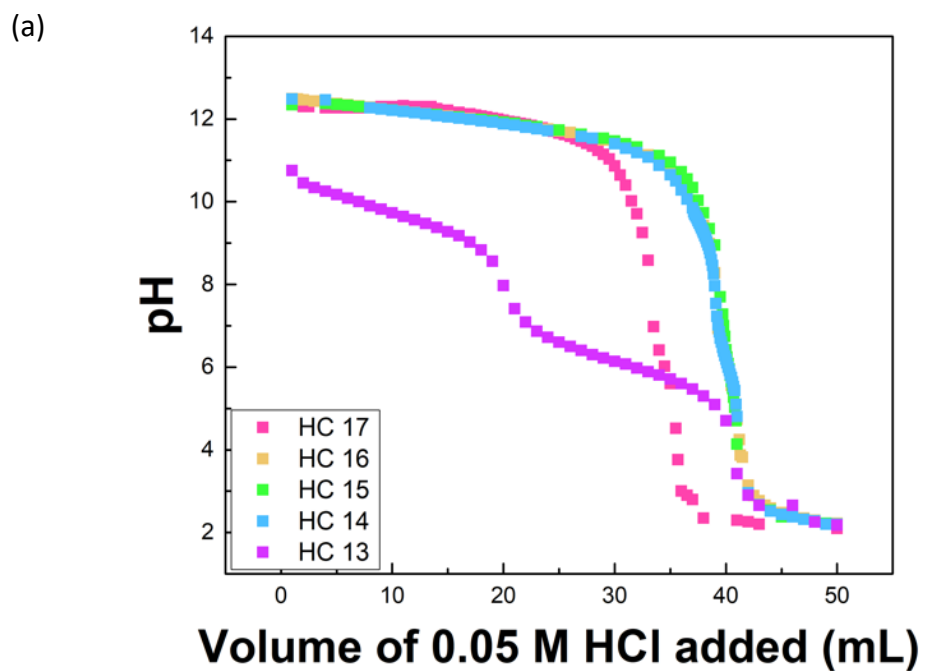
Figure 3.4. (a) The acid-base titration curves for the pH sensitive copolymers synthesized, indicating that HC 13 is not pH sensitive. (b) The pKa of polymers synthesized from different copolymer compositions.
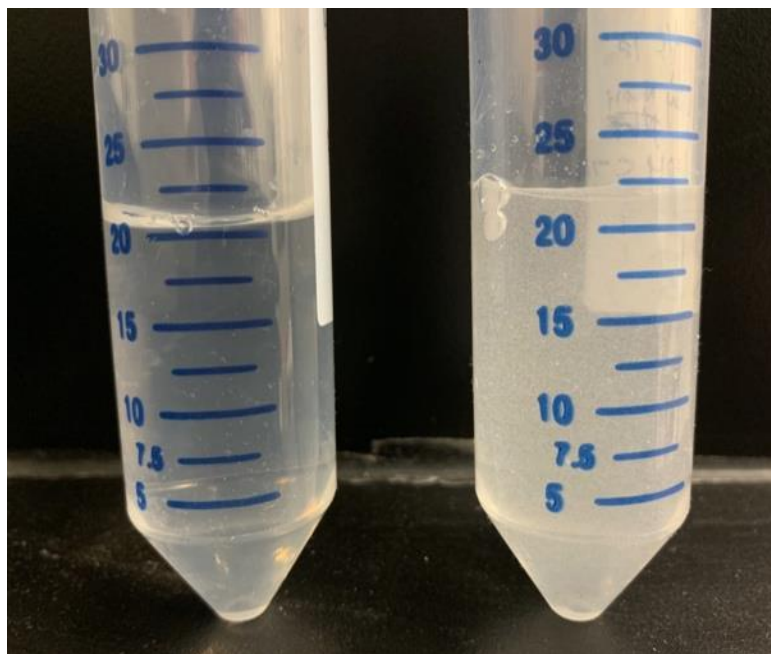
Figure 3.5. Showing the difference in dissolution properties over different pH (left Eppendorf tube-HC 14 at pH 6.9; pH>pKa, right Eppendorf tube- HC 14 at pH 6.7; pH<pKa).

Table 3.4.   The pKa values of copolymers prepared with different monomer compositions by free radical solvent copolymerisation

Sample batch	pKa
HC 13	Not pH sensitive
HC 14	6.8 ± 0.4
HC 15	6.6 ± 0.5
HC 16	5.8 ± 0.3
HC 17	5.7 ± 0.4

3.1.6. Fabrication of macropored microparticles (MPs)

Previous work has been reported to produce MPs with macropores by controlling different sonicator conditions to produce pores and/or increasing the size of existing pores of a commercial Eudragit copolymer [16,25]. In this study, we replicated similar procedures to fabricate MPs using the copolymers prepared by free radical copolymerisation of different pKa values to target specific parts of the intestine. Poly (MMA-co-MAA) has been approved by FDA as an oral drug excipient [54]. For this reason, it can be used to develop oral drug carriers. Our goal was to fabricate MPs with pH-responsive macropores using the home-made polymers.

Figure 3.6 shows SEM images of the MPs fabricated using HC 15 copolymer ((a) low magnification, (b) high-magnification). The presence of a macropore revealed the successful formation of MPs with a macropore. The resulting MPs are predominantly single-pored MPs with diameters in the range of 2-5 μm. From the image analysis using Image J software, it was found that the average size of MPs was about 2.57 ± 0.98 μm (number of particles analyzed, n = 500), as shown in the particle size distribution histogram (see Figure 3.7(a)) Figure 3.7(b) shows the histogram of pore-to-MP size ratio (i.e., the ratio of diameter of the pore to the diameter of MP) measured from MPs with unsealed macropores. As shown in the plot, it showed a bimodal distribution. In spite of the need of further research, the successful creation of these macropores can be used to enable efficient encapsulation and delivery of a wide size range of biopharmaceuticals up to around one micron.

(a)

10 µm

(b)

2 µm
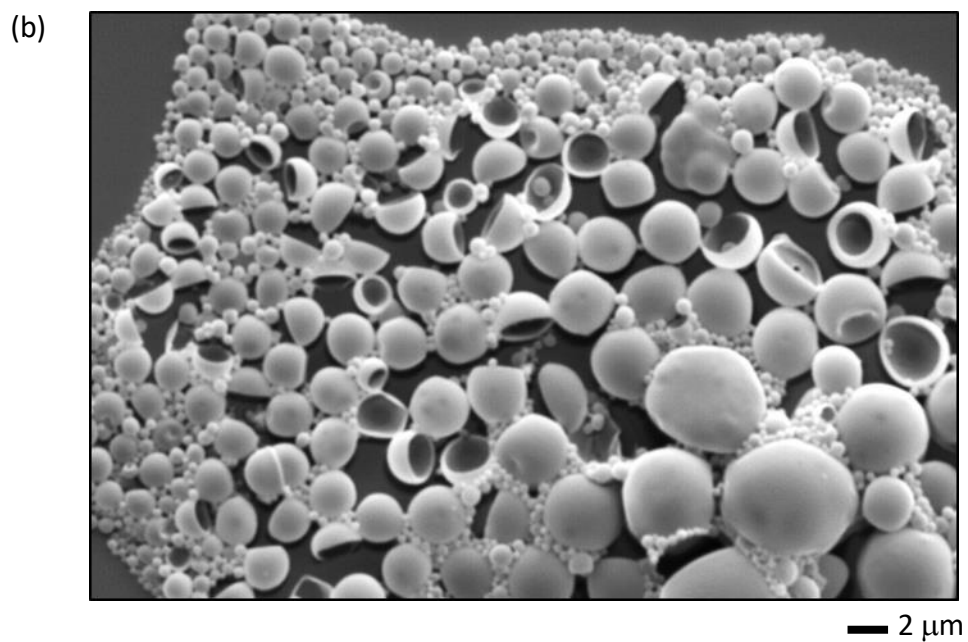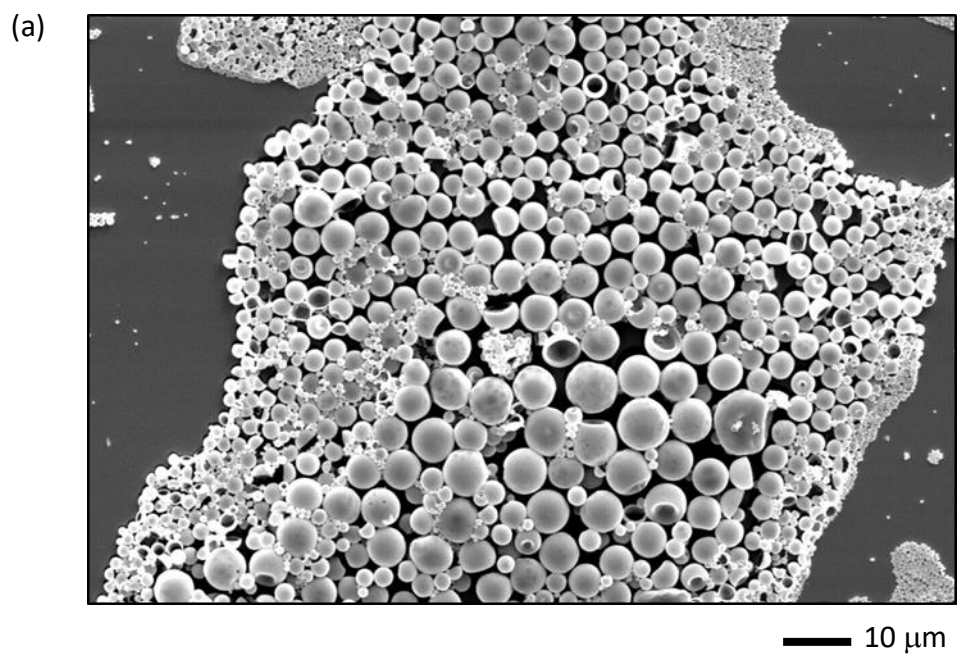
Figure 3.6. Scanning electron microscopic images of HC 15 microparticles with macropores before freeze-drying (a: low magnification, b: high magnification)

(a)

(b)
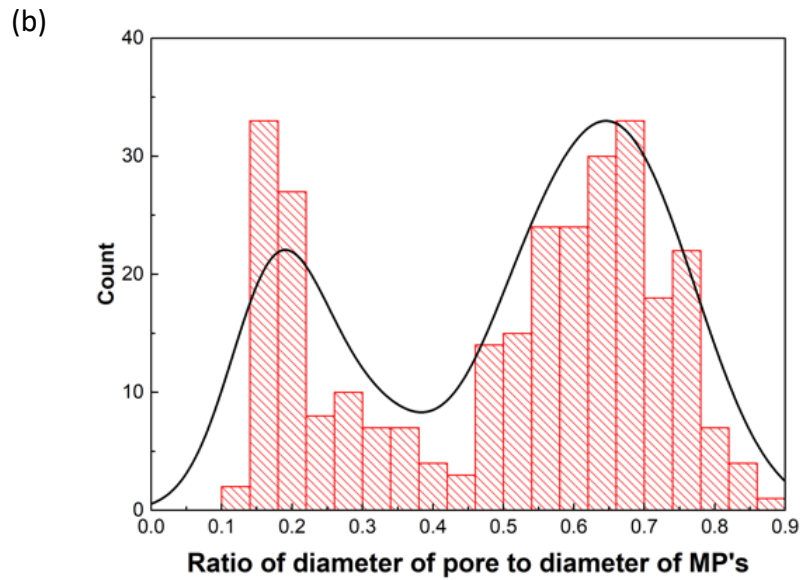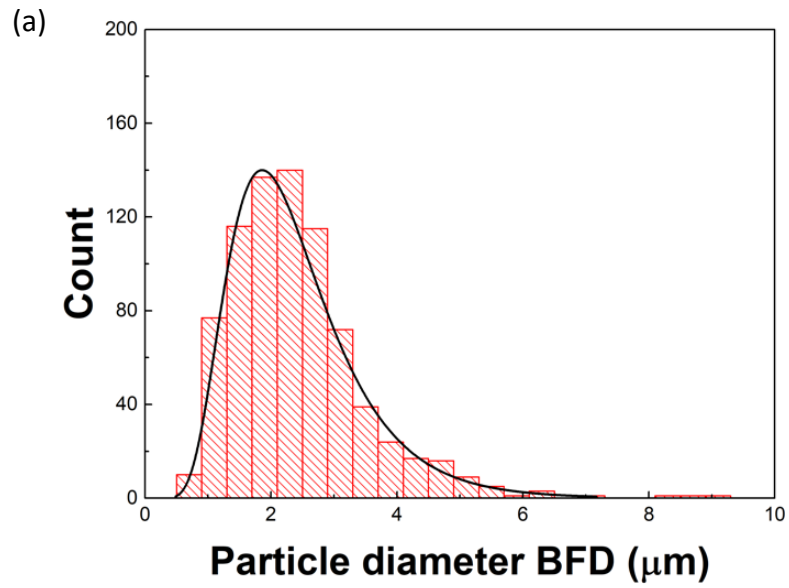
Figure 3.7. (a) Histogram of the diameter of HC 15 MPs before freeze-drying process (n = 412) and (b) histogram of pore-to-MP size ratio analyzed from SEM images (n=440).

3.1.7. Pore closure by freeze-drying

While the pores are present for the successful encapsulation of the ingredients, they must be closed after encapsulation to preserve the materials against acidic pH of stomach. To this end, we employed freeze-drying process previously developed by Ankit et al. in our group to seal the pores on MPs [16]. As shown in Figure 3.8, it is clearly evident that the freeze-drying process effectively sealed the pores of HC 15 MPs. To further support the results, SEM image analysis was performed to measure the change in the average size of MPs before and after freeze-drying. As shown in Figure 3.9, the average diameter of MPs was reduced after the freeze-drying process, as supported by SEM images before and after freeze-drying (compare Figure 3.6 with Figure 3.8) and the histogram before and after freeze-drying (compare Figure 3.7(a) with Figure 3.9). Since freeze-drying method can successfully close the pores of MPs without high temperature or the use of organic solvents, our fabrication process is clearly an advantage for encapsulation of biopharmaceuticals without destabilizing them during fabrication process.

(a)

4 µm

(b)

4 µm
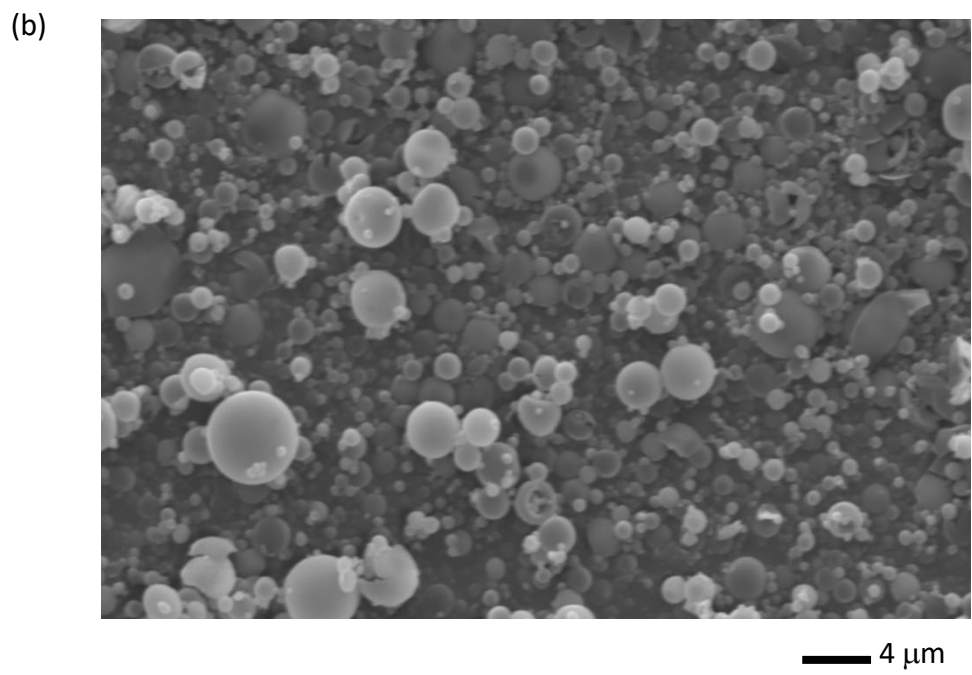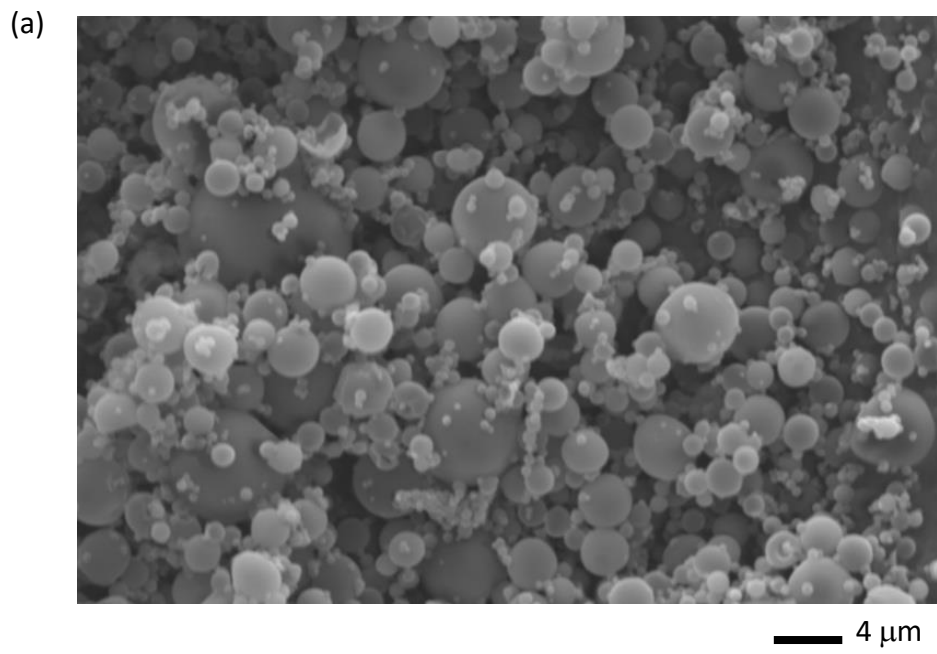
Figure 3.8. SEM images of HC 15 MPs after freeze-drying
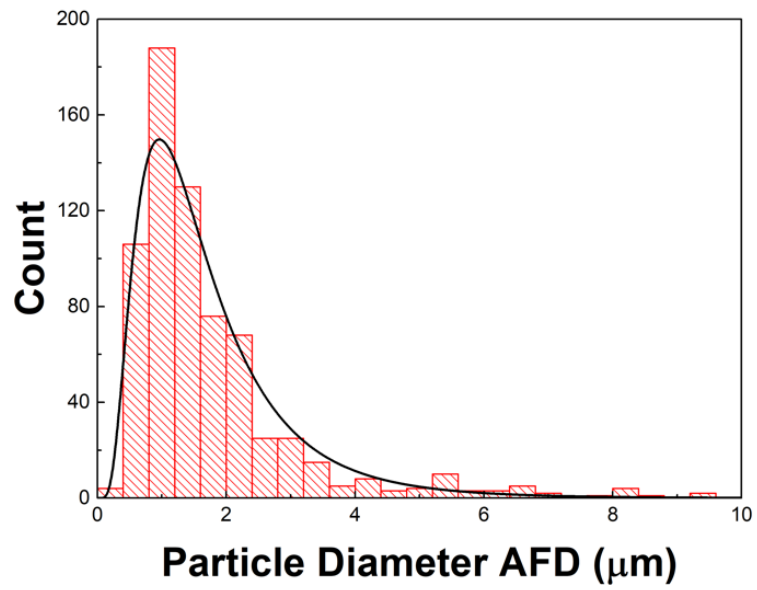
Figure 3.9. Histogram of the diameter of HC 15 MPs after freeze-drying process (n = 500)

3.1.8. Model drug-encapsulated MP formulation
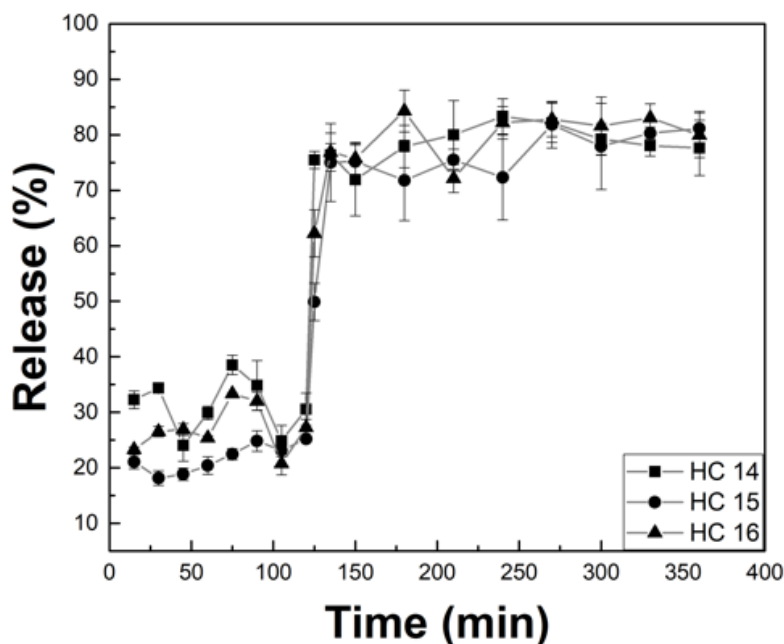
Figure 3.10. Release profile of the 100 nm fluorescent nanoparticles from MPs made of different batch copolymers. Time dependent release of FNPs from HC 14, HC 15 and HC 16 subjected to GI tract (incubation in pH 2.0 for 2 hours and pH 7.1 for 4 hours at 37 C). Release rate was calculated by measuring the relative fluorescent intensity obtained from sample at different time intervals. Complete release was achieved by vortexing the MPs with FNPs for 3 min after 4h incubation at pH 7.1 (n=4, mean ±SD)

To verify the pH-responsive pore closure/opening behavior, and to test the stability of drugs encapsulated in the pored MPs at acidic conditions, 100 nm-sized fluorescent nanoparticles (i.e., a model drug)-encapsulated MPs were prepared following the procedures described in the materials and methods section. For this purpose, three different batch polymers (i.e., HC 14, 15, and 16) were selected as they exhibited pKa values close to neutral pH. 100 nm sized nanoparticles were selected as a model drug to mimic the vaccines considering the fact that the average size of inactivated virus vaccine is around 100 nm. After encapsulation of FNPs into the MPs, it was subjected to freeze-drying process for successful pore closure. As-prepared FNPs-encapsulated

MP formulation was subjected to simulated GI tract conditions for the observation of time and pH-dependent release behavior.

The variation of fluorescence intensity was recorded at 15, 30, 45, 60, 75, 90, 105 and 120 min with the incubation time in simulated gastric fluid (SGF) for 2 hours at 37 °C, followed by 15, 30, 60, 90, 120, 150, 180, 210 and 240 min in simulated intestinal fluid (SIF) for 4 hours at 37 °C. As shown in Figure 3.10, a slight fluorescence intensity was observed during the initial incubation in SGF for 2 hours. This can be attributed to i) the leak of the FNPs from MPs with incompletely sealed pores (i.e., partially sealed pores) and ii) the release of non-encapsulated FNPs remaining in the supernatant that have not been removed completely after encapsulation. However, when the MP formulation was exposed to SIF, a significant increase in the fluorescence intensity was observed over time, saturating within few minutes. This rapid release is due to the pH-triggered opening of MP pores in the medium, demonstrating the concepted, pH-responsive MP-based oral drug formulation.

To further support the experimental results, the time-dependent release behavior of FNP-encapsulated MPs was analyzed using fluorescence microscopy. When FNP-encapsulated MPs were subjected to pH 2.0 for 2 hours, they remained intact and FNPs remained encapsulated into MPs, as shown in Figure 3.11. However, upon exposure to pH 7.1 or at a pH higher than the pKa of the copolymer, MPs showed a rapid release of FNPs due to their pore opening in response to pH change. These experiments indicate that the macropored MPs made of our anionic copolymers can encapsulate model drugs, protect them from the acidic environments in the stomach, and release them effectively in the intestine where the pH is higher than the pKa of the copolymer. Therefore, this proves that intended targeted delivery of drugs/vaccines can be achieved by synthesizing polymers of different pKa.

0 min (pH 2.0) **60 min (pH 2.0)** **120 min (pH 2.0)**

0 min (pH 7.1) **30 min (pH 7.1)** **60 min (pH 7.1)**

Control FNPs

100 μm
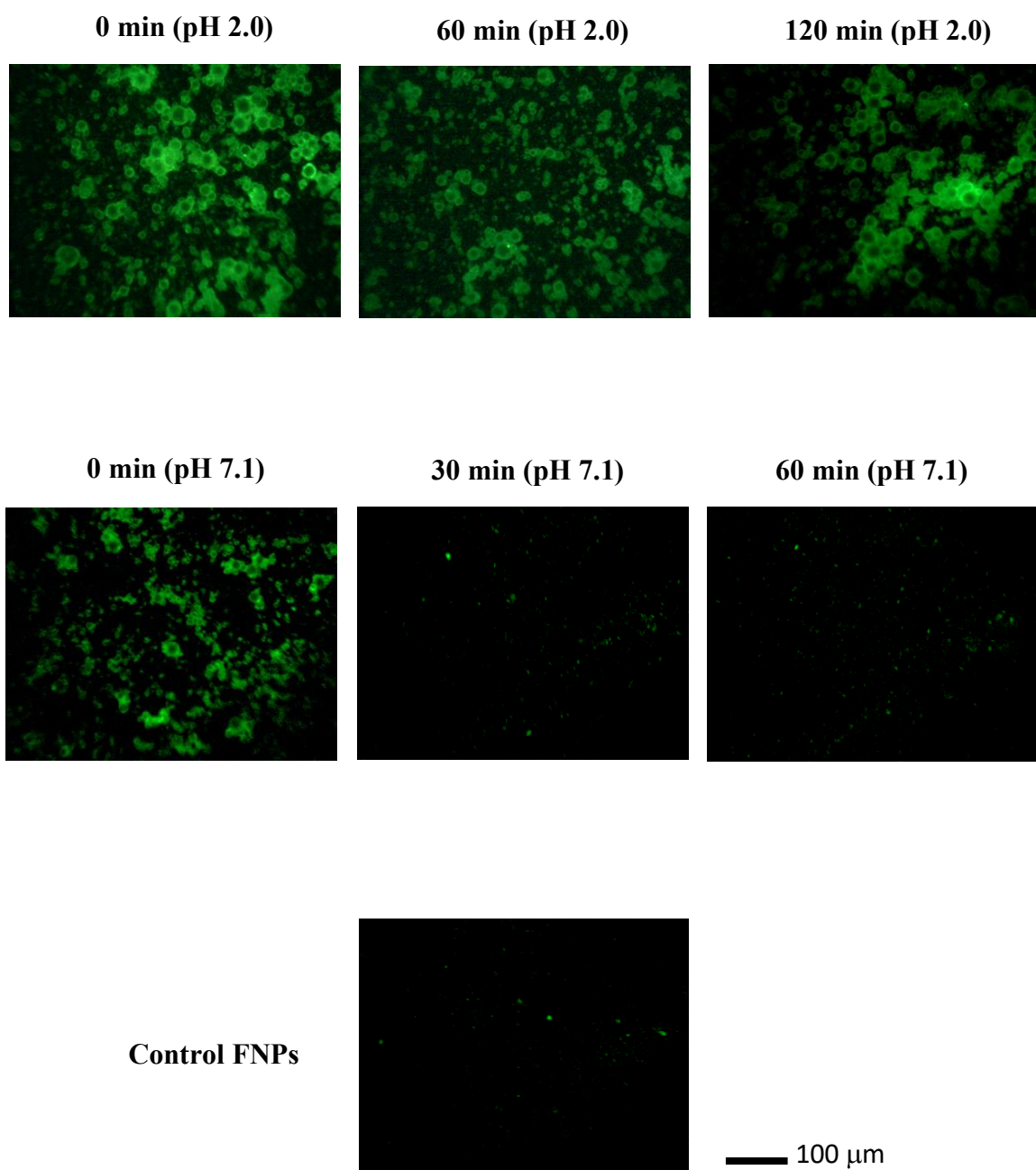
Figure 3.11. Fluorescence microscopy images of FNPs encapsulated MPs subjected to simulated gastric environments (pH 2.0) and simulated intestinal environments (pH 7.1) compared with the control FNPs (100 nm)

3.1.9. Preservation efficiency of lactase-encapsulated MP formulation

After the successful demonstration of encapsulation and release of model drug-encapsulated MPs, β-galactosidase (lactase)-encapsulated MPs were prepared to evaluate i) the preservation capability of MP formulation, indicative of therapeutic efficacy of the drug, and ii) their potential applicability in treating patients with lactose intolerance. The encapsulation of FNPs provided information about the release behavior of the MPs with a pH-responsive macropore. However, these results do not provide meaningful information in terms of the functional activity of encapsulated drugs in digestive conditions. Among several commercially available drugs, lactase was selected as a biopharmaceutical drug in this work. Since the functional and structural stability of lactase is sensitive to an acidic pH, it would lose its functional activity in gastric environment and won't regain its activity when exposed to neutral pH of intestine. Hence, it serves as a perfect drug to be tested using our pH sensitive MPs. After the encapsulation of β-galactosidase into the MPs, micro-BCA assay was conducted to find the concentration of proteins
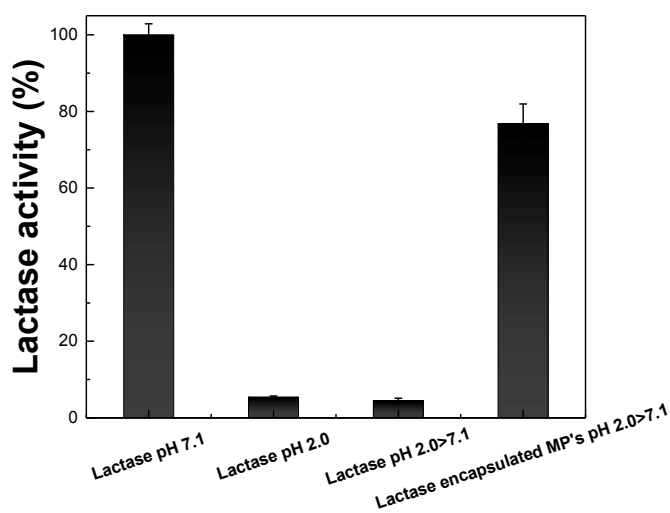
Figure 3.12. The relative remaining activity of the lactase-encapsulated into MPs subjected to GI environments (pH 2.0 incubation for 2 hours and pH 7.1 incubation for 4 hours at 37 ℃). The positive control was lactase-encapsulated MPs in pH 7.1 for 4 hours at 37 ℃. Remaining activity was also measured from lactase in pH 2.0 for 2 hours at 37 ℃ and lactase in GI environments considering to be negative control. (n=5)

encapsulated and ONPG assay was performed to determine the preservation of lactase by measuring remaining activity (see Fig. 3.12 and Fig. 3.13 for remaining activities of lactase and BCA/ONPG assays, respectively).

Micro-BCA revealed the drug loading encapsulation efficiency of the microparticles: HC 14 (3.26 ± 0.19 µg/mg of MPs, HC 15 (11.47 ± 0.60 µg/mg of MPs) and HC 16 (25.57 ± 2.53 µg/mg of MPs). For comparison of the efficacy of lactase formulations, we conducted ONPG assay of the enzyme without MP encapsulation in acidic environments (incubation for 2 hours in SGF) as negative control; in neutral environments (incubation for 4 hours in SIF) as positive control and in GI tract (incubation in pH 2.0>7.1; 2 hr incubation in SGF followed by 4 hr incubation in SIF) to confirm that lactase would not recover its functional activity. As shown in the Figure 3.12, the enzyme without MP encapsulation exhibited a significant loss/almost all of its functional activity after 2 hours of incubation in gastric environments (remaining activity: 5.4 ± 0.3%). Similarly, lactase after exposing to GI tract conditions, there was no significant remaining activity (remaining activity: 4.42 ± 0.68%). It is evident that unprotected lactase lost majority of its activity in gastric environment and does not recover when transferred to intestinal environment. In contrast, lactase-encapsulated HC 15 MPs after exposing to GI tract conditions (2 hours of incubation at 37 °C in SGF, followed by 4 hours of incubation at 37 °C in SIF) exhibited about 76.7 ± 5.21% of remaining activity, which is significantly higher than lactase without MP formulation (i.e., lactase pH 2.0>7.1). Therefore, our results indicate that close-pored MPs in the gastric condition provided a significantly higher level of protection to the encapsulated biopharmaceuticals, demonstrating potential applicability of MPs with pH-responsive macropores in developing oral drug formulations.
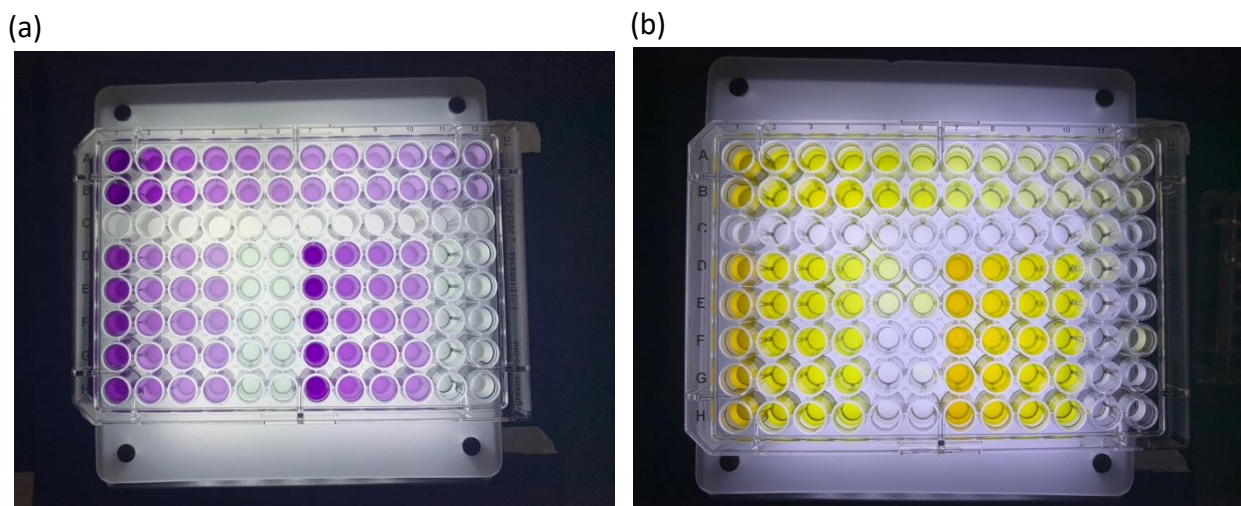
Figure 3.13. (a) Micro BCA assay plate after incubation at 37 °C for 1 hour. (b) ONPG assay plate after incubation at 37 °C for 1 hour for calculation of protein concentration and remaining activities of lactase respectively.

3.2.   Discussion

pH-sensitive polymeric MPs were designed for target-specific intestinal delivery by overcoming the commercially available polymers/delivery systems. It has been previously studied about the synthesis of poly (MMA-co-MAA) with different pKa values [58]. However, the fact that these synthesized polymers encapsulating biopharmaceuticals and protecting them from harsh environments has not been extensively researched on. Previously in our group, Ankit et al. have researched and discovered a new microencapsulation of biopharmaceuticals using commercially available polymers and have been successful in demonstrating preservation and encapsulation of drugs. In this work, we extended the research to synthesize a library of anionic copolymers with different pKa values, which can further be used for target-specific delivery of different kinds.

Free-radical polymerisation was employed to synthesize poly (MMA-co-MAA) copolymers. The structure and composition of copolymers were investigated by FTIR and NMR.

Using results from FTIR, it was analysed with increase in mol% of MAA in the copolymer, there was a significant increase in the peaks in the range 2500 to 3500 cm^{-1}. The copolymer compositions were calculated using the spectra obtained from proton NMR and the molecular weights by GPC. In this work, pH-responsive copolymeric MPs with macropores were fabricated and methods were employed to successfully encapsulate biopharmaceuticals by freeze-drying process through pore closure. We also conducted ONPG analysis to determine the remaining activity of the enzyme after exposing the real drugs encapsulated in MPs to simulated gastric environments followed by their release in the intestine. The production of MPs with macropores were confirmed by SEM analysis. Further, they were then subjected to freeze-drying which induced the closure of pores as proven by SEM analysis. While the detailed mechanism has not been studied, pore-closure might be associated with intra-mass transfer in polymeric MPs without damaging the hollow interior [25].

The successful closure of the MP pores enabled the application of the MP-based oral drug formulation by protecting the ingredients in the harsh gastric environments. In addition to pore-closure, they tend to open pores at near neutral pH (above its pKa), making them not only protect the drugs form the harsh gastric environments but also releasing them at target-specific sites in the intestine. As a result, lactase-encapsulated MPs from different batches were effective and efficient in protecting lactase and preserving its activity in pH 2.0, leading to almost 17 times higher than lactase without MP encapsulation in the GI tract. In this work, digestive enzymes were not used in preparing SGF and SIF due to the difficulty of separating lactase from the lactase-digestive enzyme mixture. Importantly, the presence of digestive enzymes would interfere with BCA and ONPG assay results. While not performed in this work, it is expected that our polymer would behave in a similar way in simulated digestive conditions with digestive enzymes such as pepsin and pancreatin.

In conclusion, the pH-sensitive MPs fabricated using different pKa polymers provides solutions to improve control over pH-dependent release of drugs at the targeted sites. Considering the major technical challenges of oral drug delivery, our MPs can be used as a potential alternative to the current delivery systems. Further, by encapsulating mucolytic enzymes into MPs as researched previously by Bahman et al, we can even increase the adhesion and penetration of drugs through the mucous layer at the targeted sites.

4. Results and discussion (Microneedles)

4.1. Fabrication of CNC microneedles

Figure 4.1 shows SEM images of the first generation PDMS molds. It clearly shows the formation of conical needle structures, as evidenced by the cavity of microneedles in the PDMS mold (low-magnification: Figure 4.1(a), high-magnification: Figure 4.1(b)). The PLA replica has been fabricated using the high quality PDMS molds (see Figure 4.2 for the bright field microscope images and Figure 4.3 for SEM images, respectively). PLA replicas were cast from PDMS molding, and the length and base diameter of the needles were measured to be 400 ± 20 µm and 300 ± 15 µm, respectively.
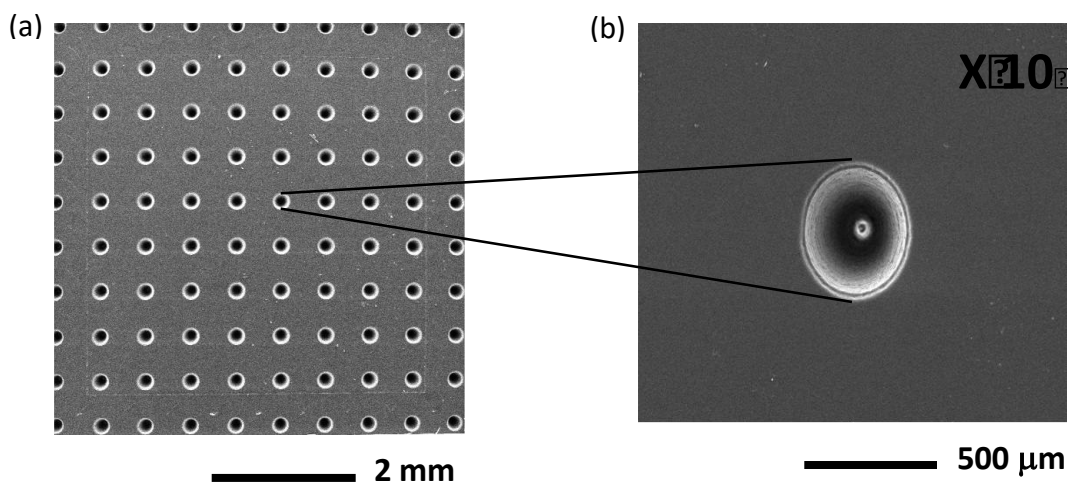
Figure 4.1. PDMS negative molds observed under SEM. (a) 10×10 structure of the entire negative PDMS molds. (b) Zoom-in image of a microneedle structure

Formulations composed of CNC along with the model drug (FNPs) in trehalose + CNC were used to make CNC microneedle patch from PDMS molds (see Figures 4.4 (a)-(c) for SEM images, Figure 4.4(d) for optical microscope images, and Figure 4.4(e) for fluorescence microscope images). SEM and optical microscopy analysis confirm the fabrication of quality CNC

microneedles (sharpness: 16±2 μm) with a clear precision with 400±20 μm in length without any

significant defects on their surface.
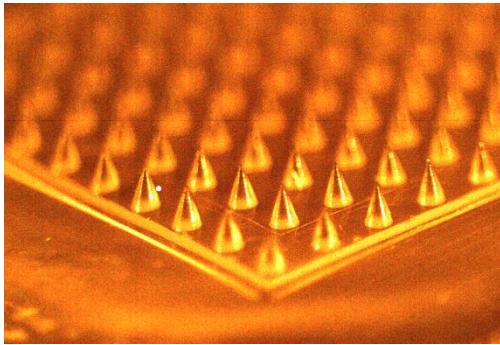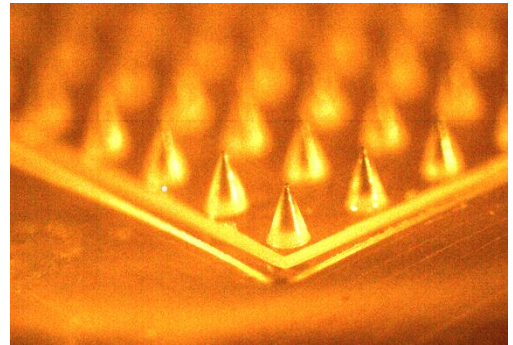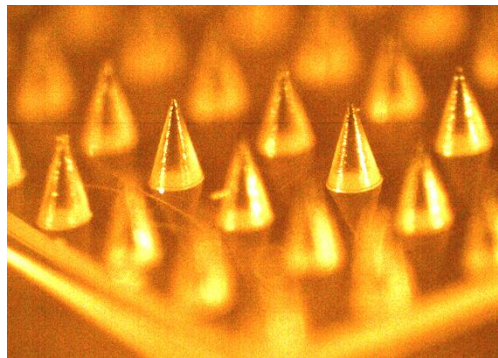
Figure 4.2. The bright field microscopy images of the PLA positive molds replicating the aluminum master made from first generation PDMS negative molds by micromolding process.

(a)

200 µm

(b)

100 µm

(c)

40 µm
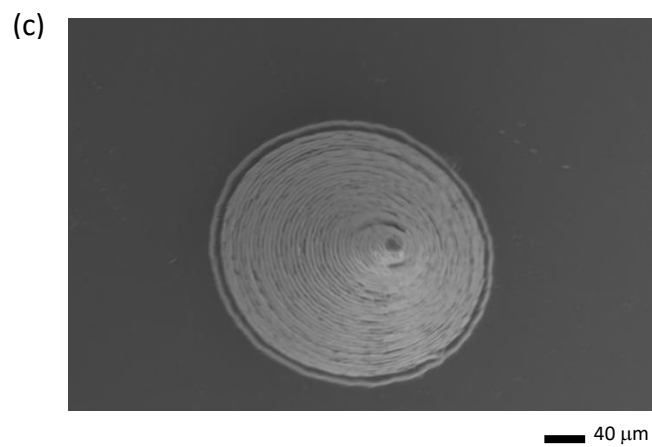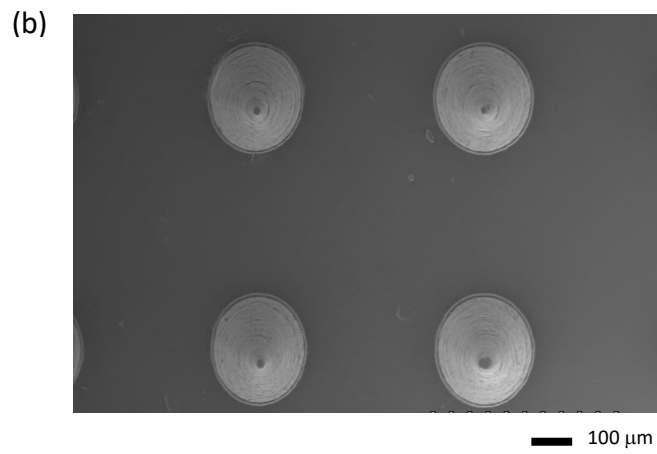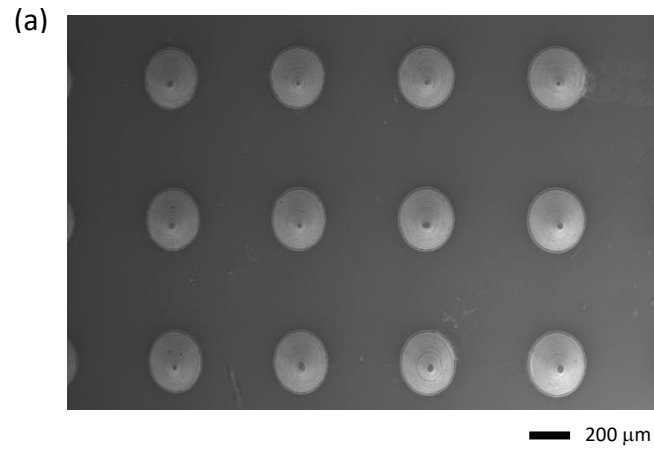
Figure 4.3. SEM images of PLA microneedles synthesized by micromolding process from first generation PDMS mold, 55X (a), 150X (b), and 350X (c).
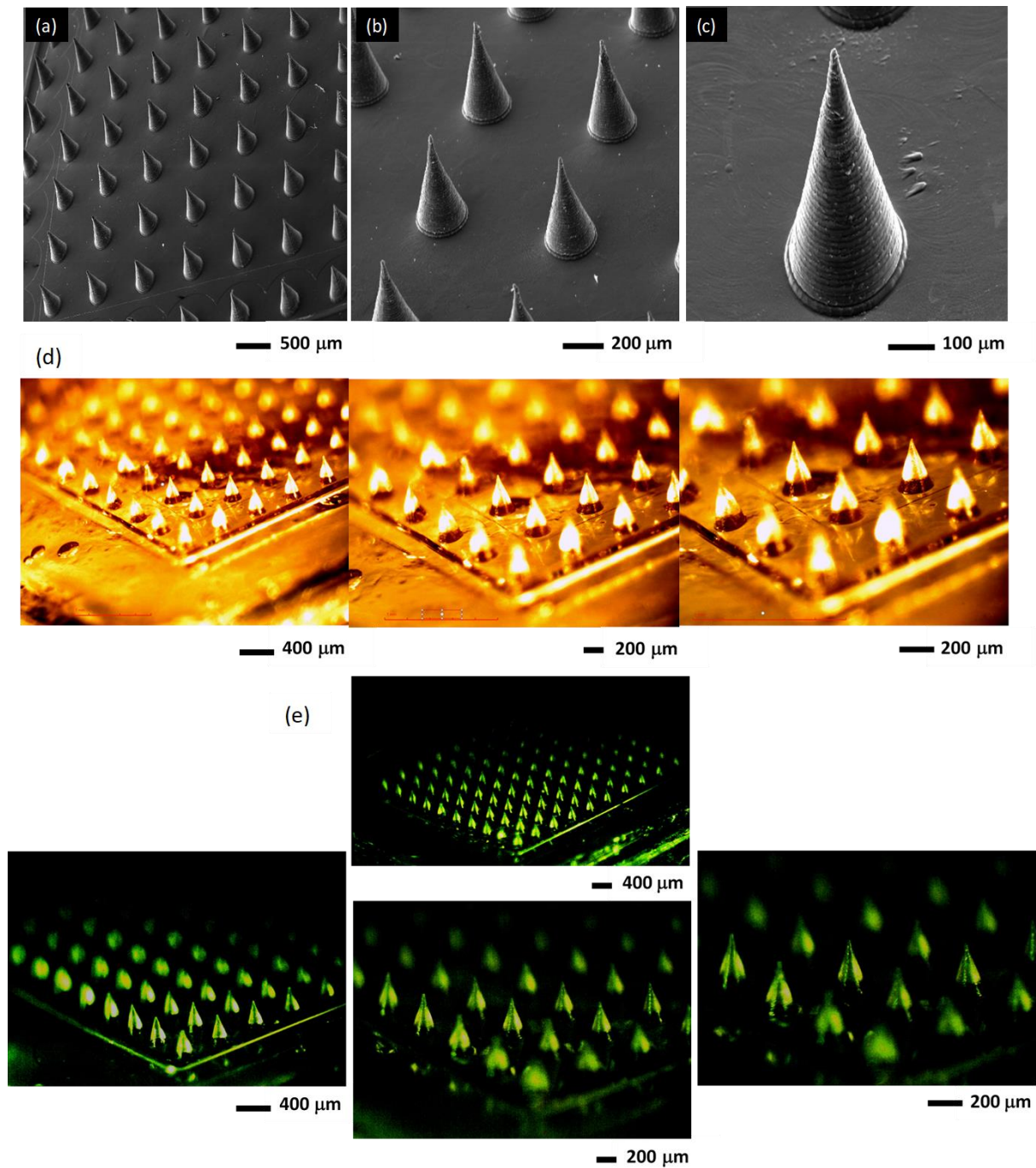
Figure 4.4. CNC microneedles fabricated by micromolding process. (a), (b), (c) SEM images of CNC microneedles fabricated from PDMS molds of different magnifications. (d) Optical microscopy images of CNC microneedles. (e) Fluorescence microscopy images of FNPs (100 nm)-encapsulated CNC microneedles

4.2. Studying the viscosity of formulations

Different concentrations of CNC formulations were prepared for their application to the fabrication of microneedles. It has been reported that crystallization and phase-separation of microneedle formulation play a critical role in destabilization of biopharmaceuticals [95]. In order to maintain the stability of the vaccines during fabrication and storage of drug-encapsulated microneedles, our goal was to control the viscosity of the formulation and thus to suppress the phase-transformation of the sugar-based solid microneedles [91]. As expected, with higher concentrations of cellulose nanocrystals, the viscosity of the microneedle formulations kept increasing (see Table 4.1). From the conducted experiments, the control formulation (trehalose + CMC) exhibited viscosity around 5.53 ± 0.7 cp. As shown in the Table 4.1, it is observed that 0.75% (w/w) CNC formulation had similar viscosity to the control formulation.

Table 4.1. Different formulations and their respective viscosities measured by rheometer

Sample condition	Viscosity (cp)	±SD
Control (15% Trehalose+0.5% CMC)	5.53	0.7
15% Trehalose + 0.1% CNC	2.13	0.8
15% Trehalose + 0.25% CNC	2.32	0.5
15% Trehalose + 0.5% CNC	3.86	0.4
15% Trehalose + 0.75% CNC	5.14	0.6
15% Trehalose + 1% CNC	9.16	0.5
15% Trehalose + 2.5% CNC	64.52	4.6

4.3. Minimum force required for insertion of microneedles into pig ear skin

As the microneedles were fabricated to deliver biopharmaceuticals/vaccine to animals (such as pig), we investigated the minimum force required to insert the microneedles into pig tissue sample. The pig ear tissue was isolated and kept on a flat base. The moving end had 400 μm PLA molds attached using epoxy glue. The rheometer test geometry was set to move axially downwards at 2 μm/s for the needles to get in contact with the tissue. As shown in Figure 4.5, it is evident that the minimum force required for insertion of the microneedle patch is approximately 7.8 ± 0.4 N.
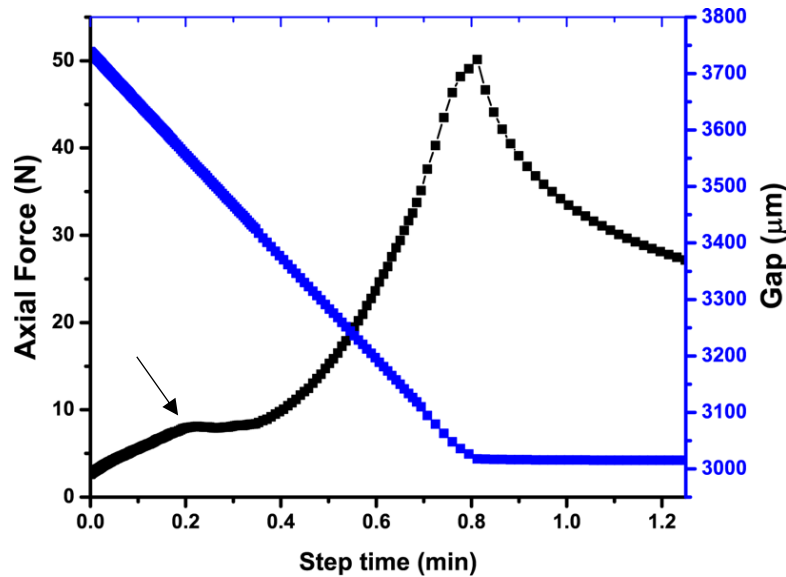
Figure 4.5. The graphical representation to determine the minimum force required for insertion through the pig ear tissue by 10×10 microneedles of 400 μm length.

4.4. Mechanical strength analysis

Force vs. displacement graph was recorded from the software linked to the rheometer to measure mechanical strength of CNC microneedles. For each microneedle patch, the rheometer pressed an array of microneedles against a rigid metal surface as shown in Figure 4.6. It was observed that the force suddenly dropped on needle failure. The maximum force applied immediately before its drop was interpreted as the force required for microneedle failure. The

58

CMC backing is brittle after drying causing the backing to break before the needles getting compressed/break. The data were discarded if the backing shattered instead of the needles being damaged. As shown in Figures 4.7 and 4.8, the conventional sugar-based microneedles (i.e., trehalose + CMC formulation) exhibited 3.6 ± 2.2 N as the breaking force, which is smaller than the minimum force required for penetration through pig skin tissue. However, CNC-based microneedles showed greater mechanical strength compared to the control microneedles. For example, 0.05% (w/w) CNC microneedles had about 9 N, which was higher than the minimum force required for insertion and almost two-fold increase of mechanical strength compared to the control microneedles. It was further observed that with the increase in concentration of CNC in the microneedles, the mechanical strength also increased until it started saturating from 1% (w/w) to 2.5% (w/w) CNC microneedles, as shown in the Figure 4.8 and Table 4.2. This proves that CNC microneedles have higher mechanical strength than control microneedles and higher failure force than the minimum force required for insertion into pig skin tissue. It should be noted that the 0.75% (w/w) CNC microneedles exhibited the failure force 23 ± 4 N which is significantly higher than the minimum force required to pierce through the skin tissue.

Most of the microneedles were compressed after mechanical strength tests. Figure 4.9(a) shows the microneedle image before mechanical strength tests, while Figures 4.9 (b), (c), (d), (e), and (f) show the images after mechanical tests. As shown in the optical microscopy images, the microneedles were clearly bent/smashed in account with the force applied by a rheometer, which is consistent with SEM images (Figures 4.9 (b)-(f) and 4.10).
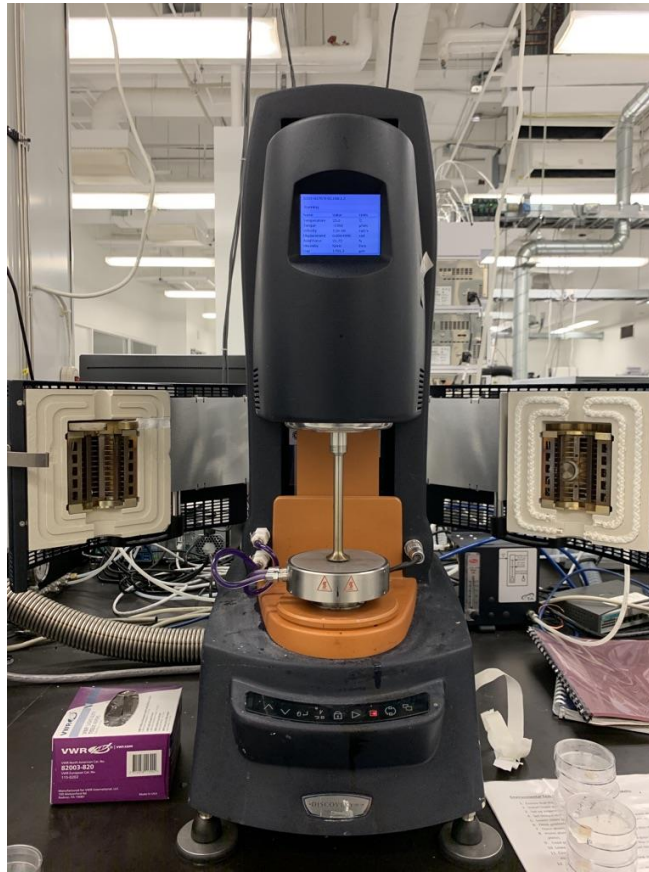
Figure 4.6. The image of the HR 2 rheometer by TA instruments used for characterisation of the failure force of microneedles
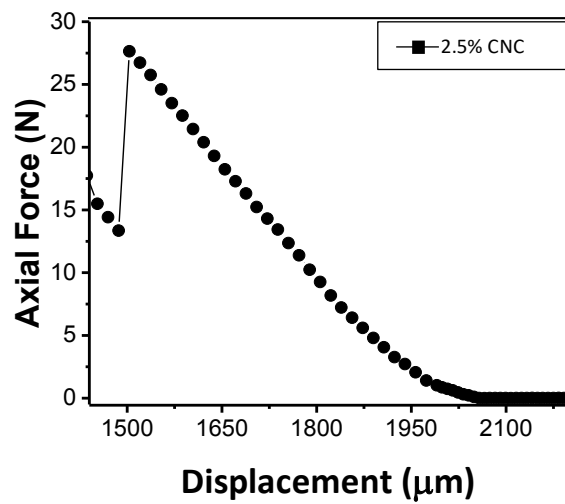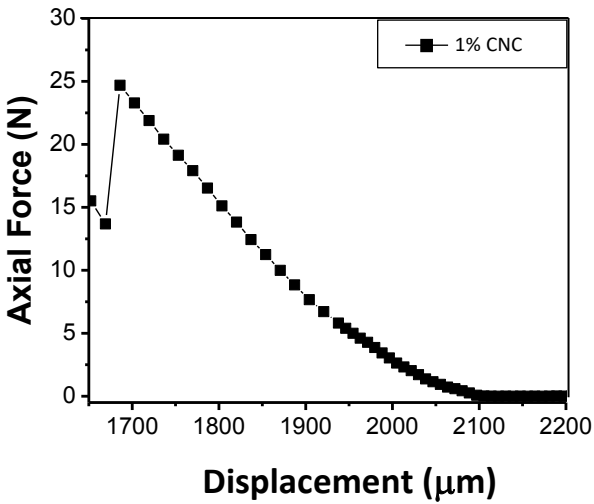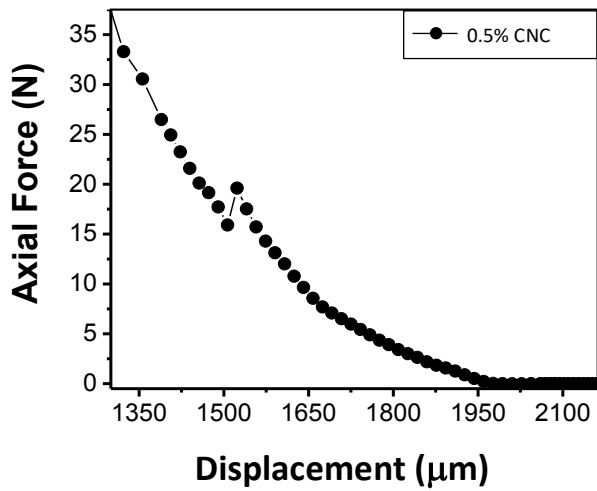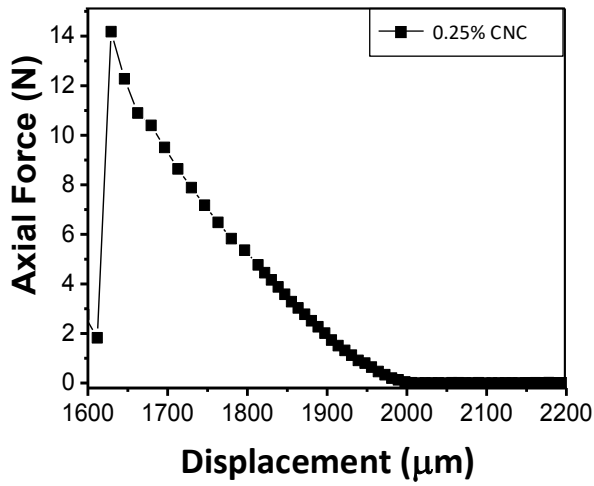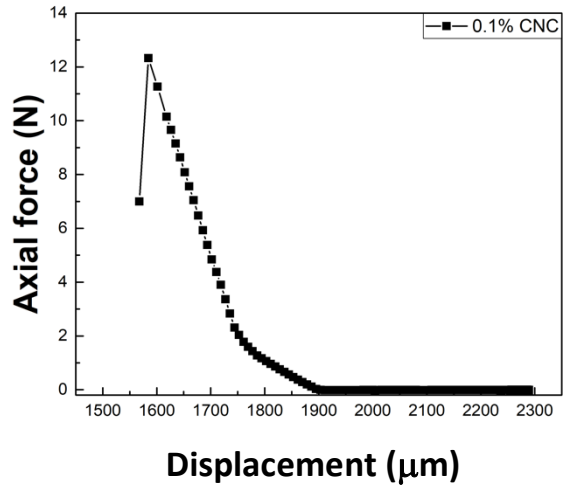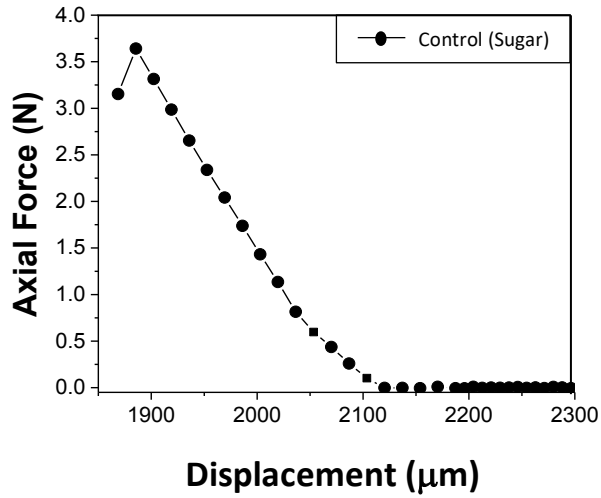
Figure 4.7. Mechanical force versus gap (displacement) data for different wt% of CNC microneedles. The point at which the force suddenly drops is considered the failure force for the microneedles.

61
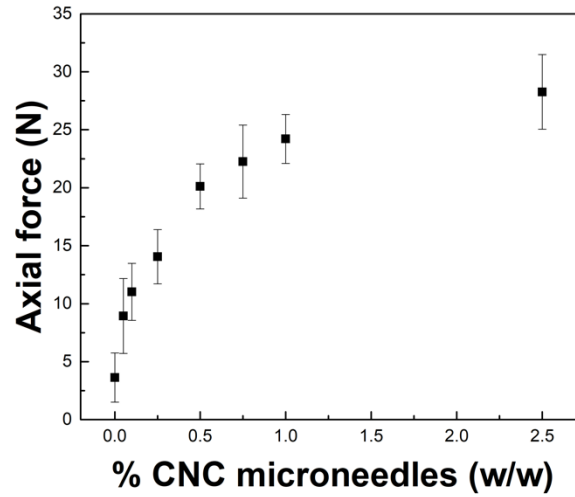
Figure 4.8. The range of mechanical strength of CNC microneedles.

Table 4.2. Failure force of microneedle patch with different amounts of CNC. With increase in concentration of CNC the needles tend to have higher mechanical strength.

CNC (wt%)	Failure force (N)	$\pm SD$
0	3.62	2.12
0.05	8.94	3.23
0.1	11.02	2.45
0.25	14.05	2.34
0.5	20.12	1.94
0.75	22.25	3.15
1	24.21	2.11
2.5	28.26	3.21
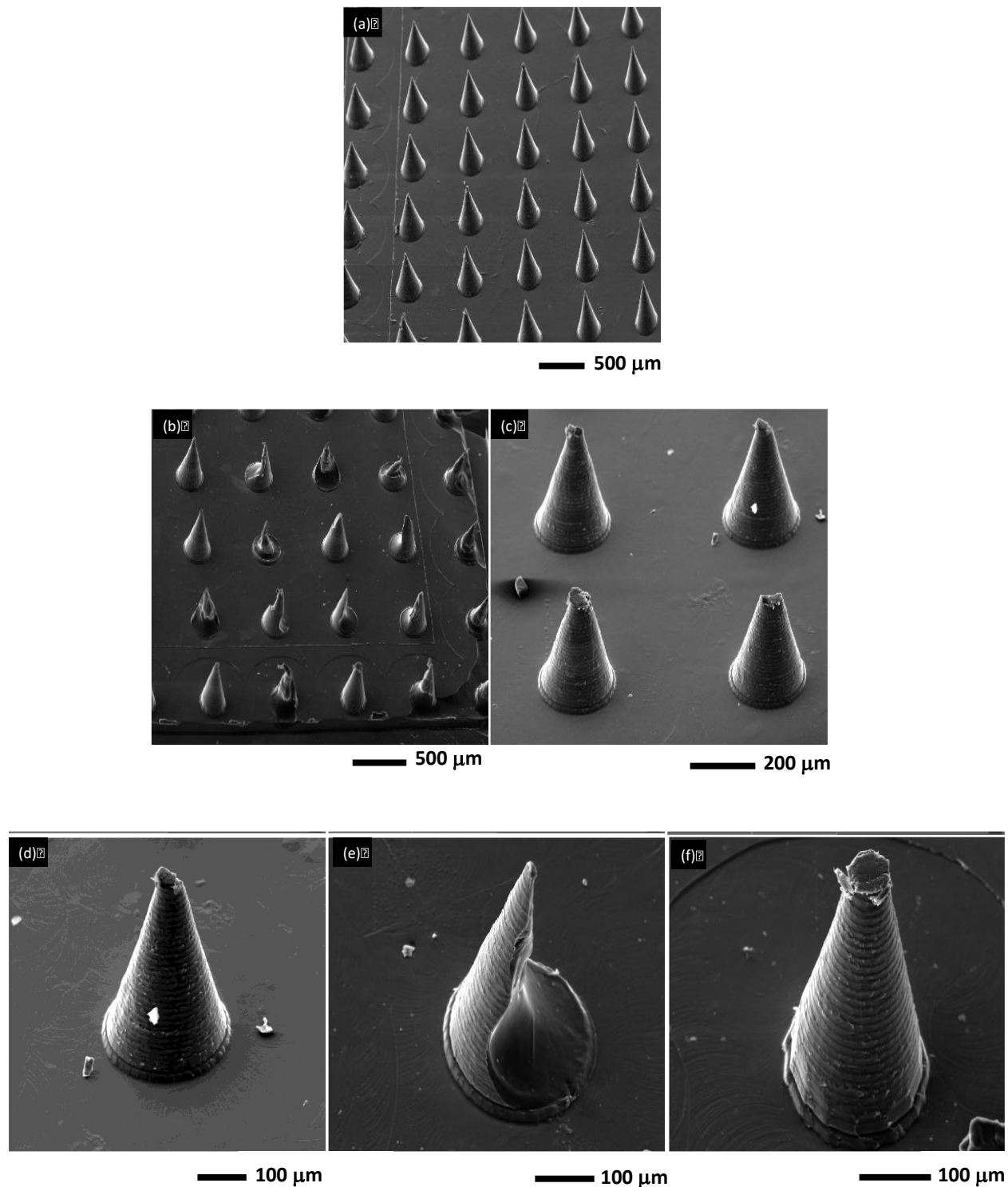
Figure 4.9. (a) SEM of CNC microneedles before mechanical strength tests. (b), (c), (d), (e) and (f) are the SEM of CNC microneedles after mechanical strength analysis. The needles are shattered, broken completely or compressed.
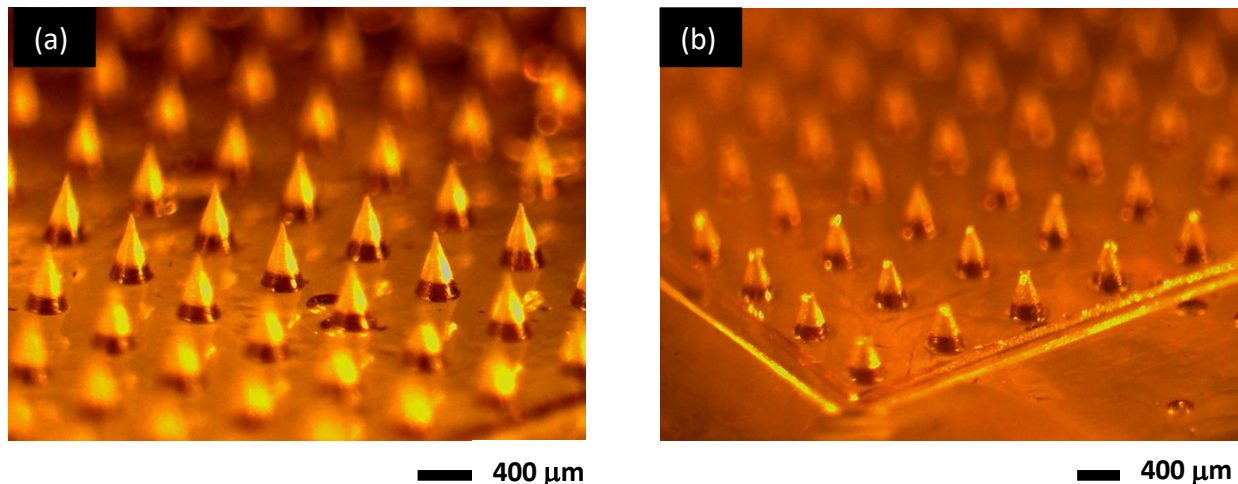
Figure 4.10. (a) Optical microscopy image before mechanical strength analysis. (b) Compression and breaking of needles after mechanical strength tests of the microneedles.

From the measured mechanical properties of microneedles, the 0.75% (w/w) CNC microneedles were predicted to be strong enough to penetrate the pig skin tissue. In addition, the measurement of a similar level of viscosity as the control microneedle formulation would effectively prevent phase transformation-induced destabilization of microneedle drugs/vaccines based on the previous report [91]. While high viscosity can be effective in suppressing phase transformation, it should be noted that the CNC formulation cannot provide protection to the solid microneedles against ambient moisture, which is critical for the long-term and environmental stability of microneedles. Considering the importance of a protection against moisture, we came up with an idea of forming a moisture-proof coating on to the surface of microneedles using an anionic pH-sensitive copolymer, i.e. Eudragit S100. To this end, coating thickness was varied by controlling the coating time of the spray station (i.e., 1, 2, 5, and 10 sec), and thus 0.75% CNC microneedles with four different thick protection layers were fabricated.

Figure 4.11 shows that with the increase in time, the thickness of the polymer on the CNC microneedles kept increasing. Optical microscopy images show that a uniform protection layer was formed on the surface of the microneedles at coating times < 10 sec (Figure 4.12). Although

environmental stability test has not been performed in this work, it is reasonable to assume that thicker coating would better protect moisture-sensitive interior microneedle drugs/vaccines. Also, protection layer may further increase mechanical strength of the microneedles compared to that of the control microneedles. To this end, mechanical tests have been performed to characterize the effects of protection coating on the failure force of microneedles. As expected, the failure force of the microneedles increased with increasing polymer coating thickness (or time) (see Figures 4.13 and 4.14, and Table 4.3). From the analysis of the force vs displacement curves, a significant increase in the strength of CNC microneedles was observed from coating times > 2 seconds.
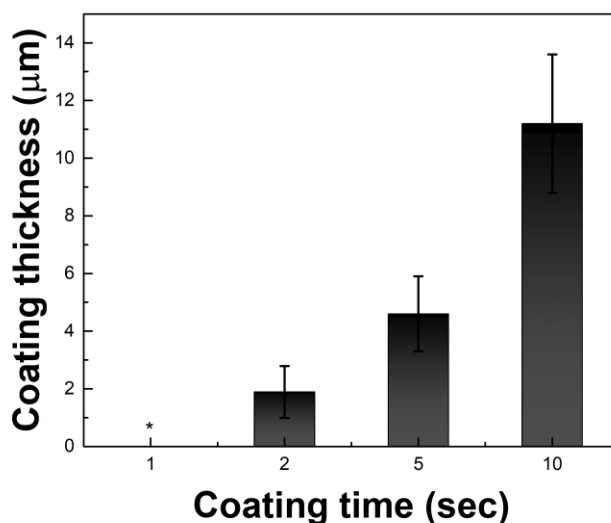
*Figure 4.11. Relationship between thickness of the protection layer and coating time. * Thickness was not consistent.*

1 second

Before coating

2 seconds

— 200 μm

5 seconds

10 seconds

— 200 μm
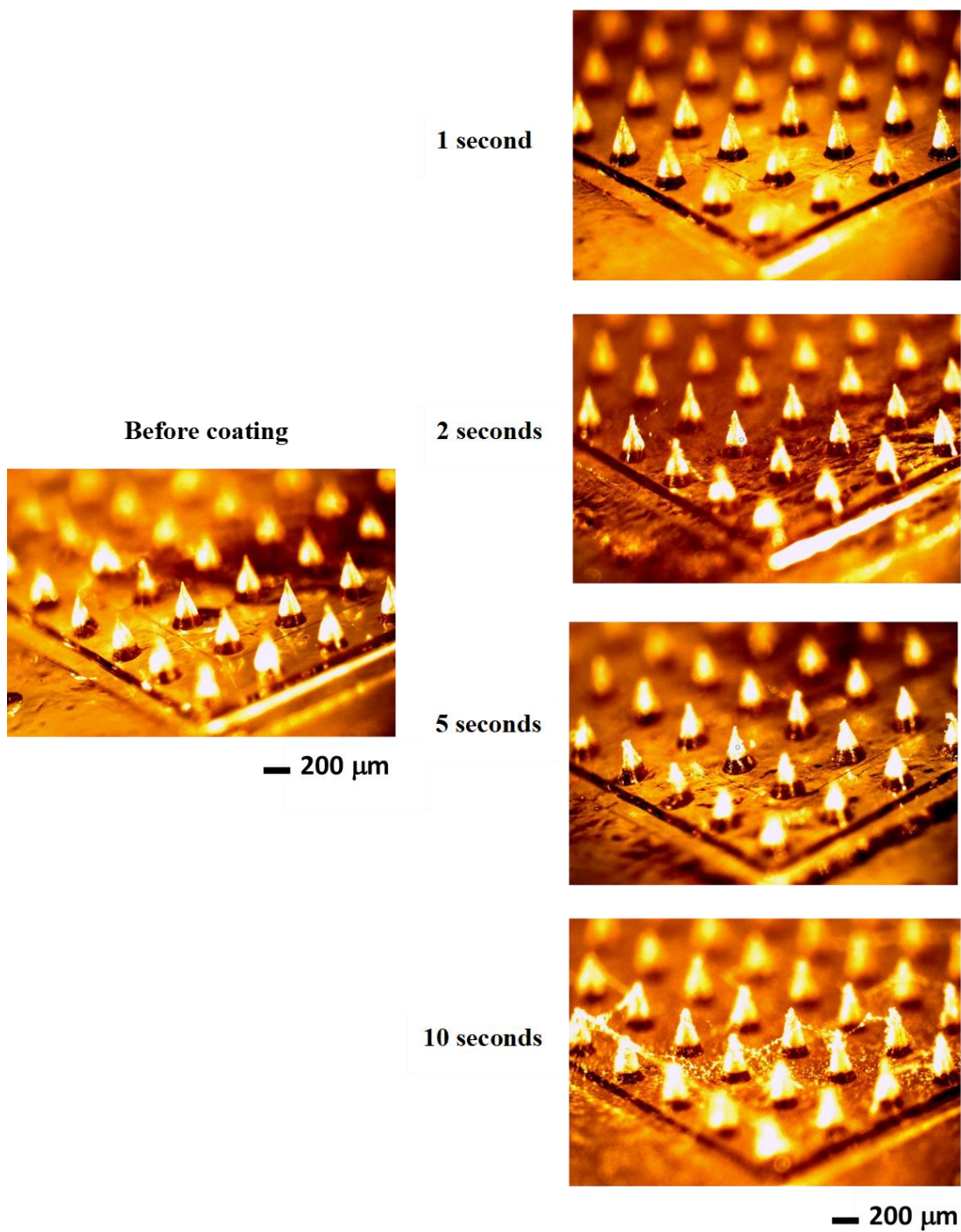
Figure 4.12. Optical microscopy images of the 0.75% CNC microneedles before and after coating with Eudragit S100 polymer by spray coating of different time exposures.
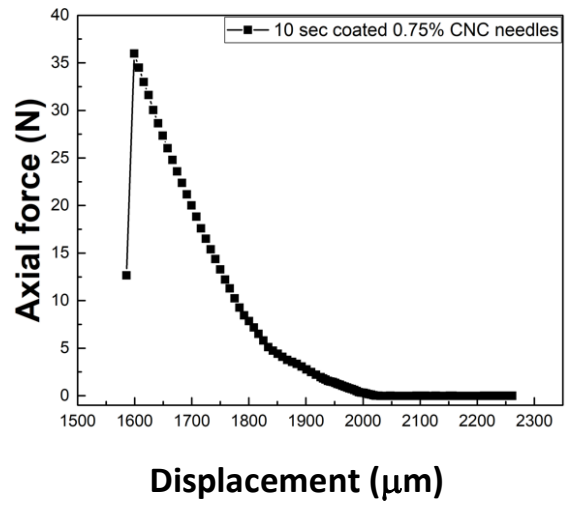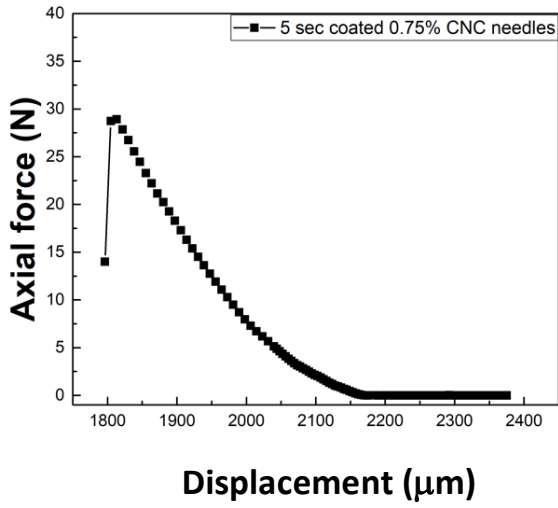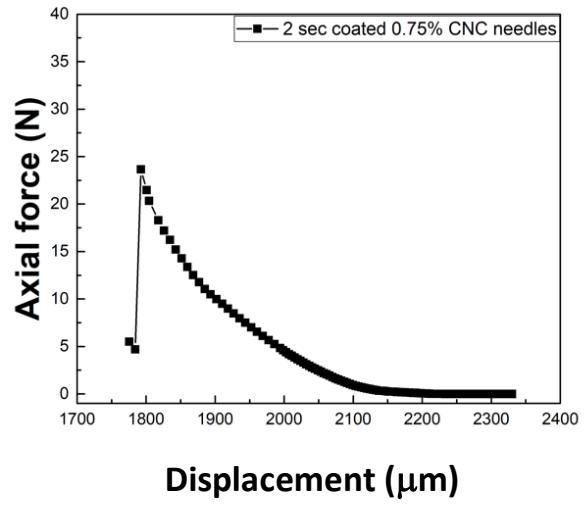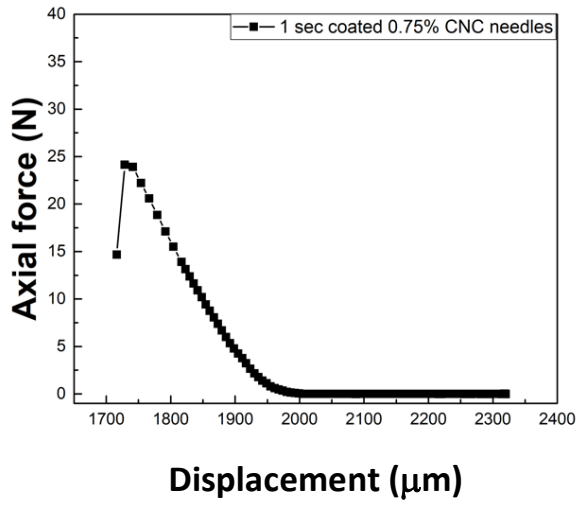
Figure 4.13. 0.75% CNC microneedles subjected to different exposure times for spray coating S100 Eudragit- The relationship between axial force and displacement
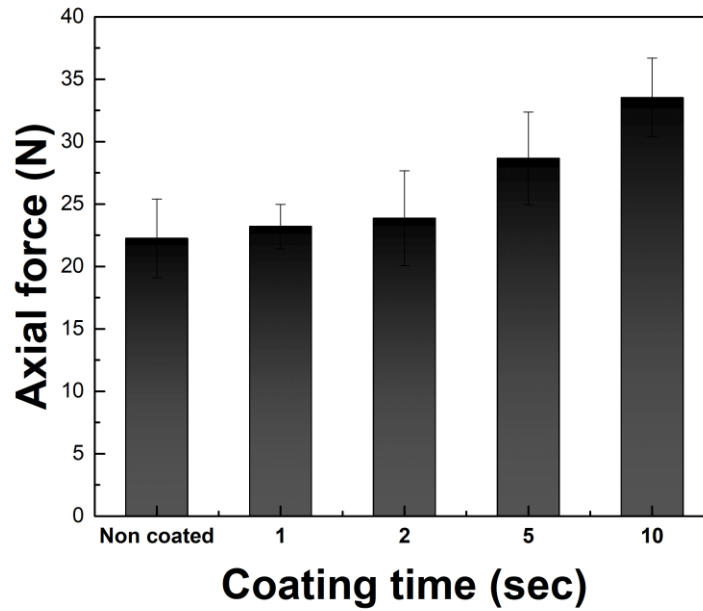
Figure 4.14. Axial force vs. coating time. The failure force increases with increase in the exposure of time during spray coating process

Table 4.3. Axial force vs. coating time

Time coated (s)	Failure force (N)	±SD
Non-coated	22.25	3.15
1	23.2	1.78
2	23.87	3.8
5	28.66	3.72
10	33.53	3.157

4.5. Insertion of microneedles into pig skin tissue

The 10×10 array of 0.75% CNC microneedles were inserted gently into the skin by compression with a thumb. They were held onto the skin for 10-15 seconds. The tips of the needles have been dissolved as soon as they were inserted into the skin, indicating the rapid dissolution of the CNC formulations in the skin (Figure 4.15). After removing the microneedle patch, the skin was treated with a tissue marking dye (stained for 5 minutes), followed by cleaning with isopropanol to remove unreacted dye on the tissue surface (Figure 4.16). The observation of the dye-stained markings on the skin demonstrates the successful penetration of the microneedles into the pig skin tissue (Figures 4.16 (d) and (e)).

400 µm
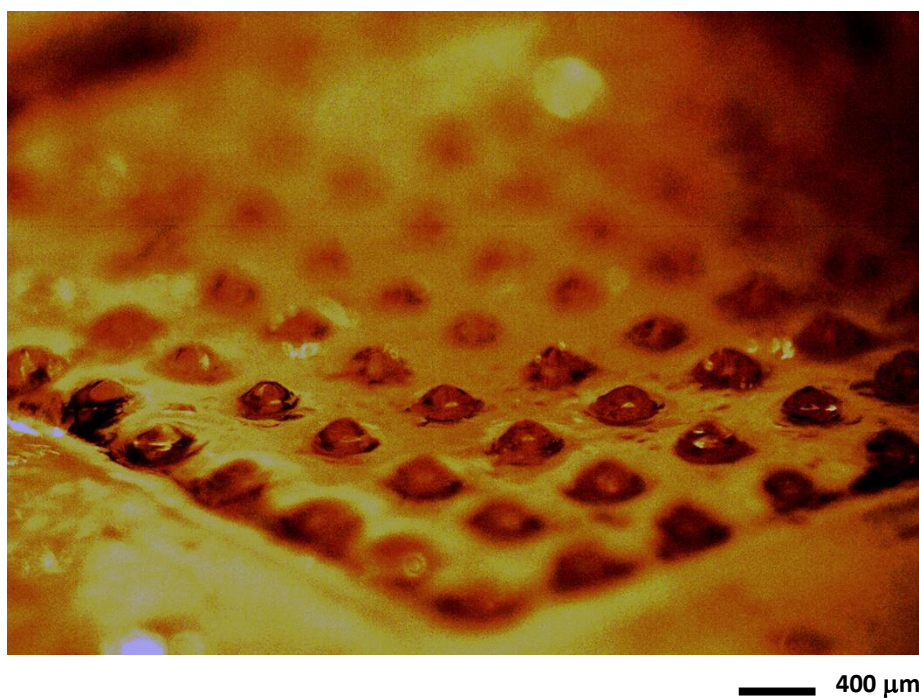
Figure 4.15. Optical microscope image of 0.75% CNC microneedles after pig skin insertion test. The needles are dissolved while the backing remaining intact.
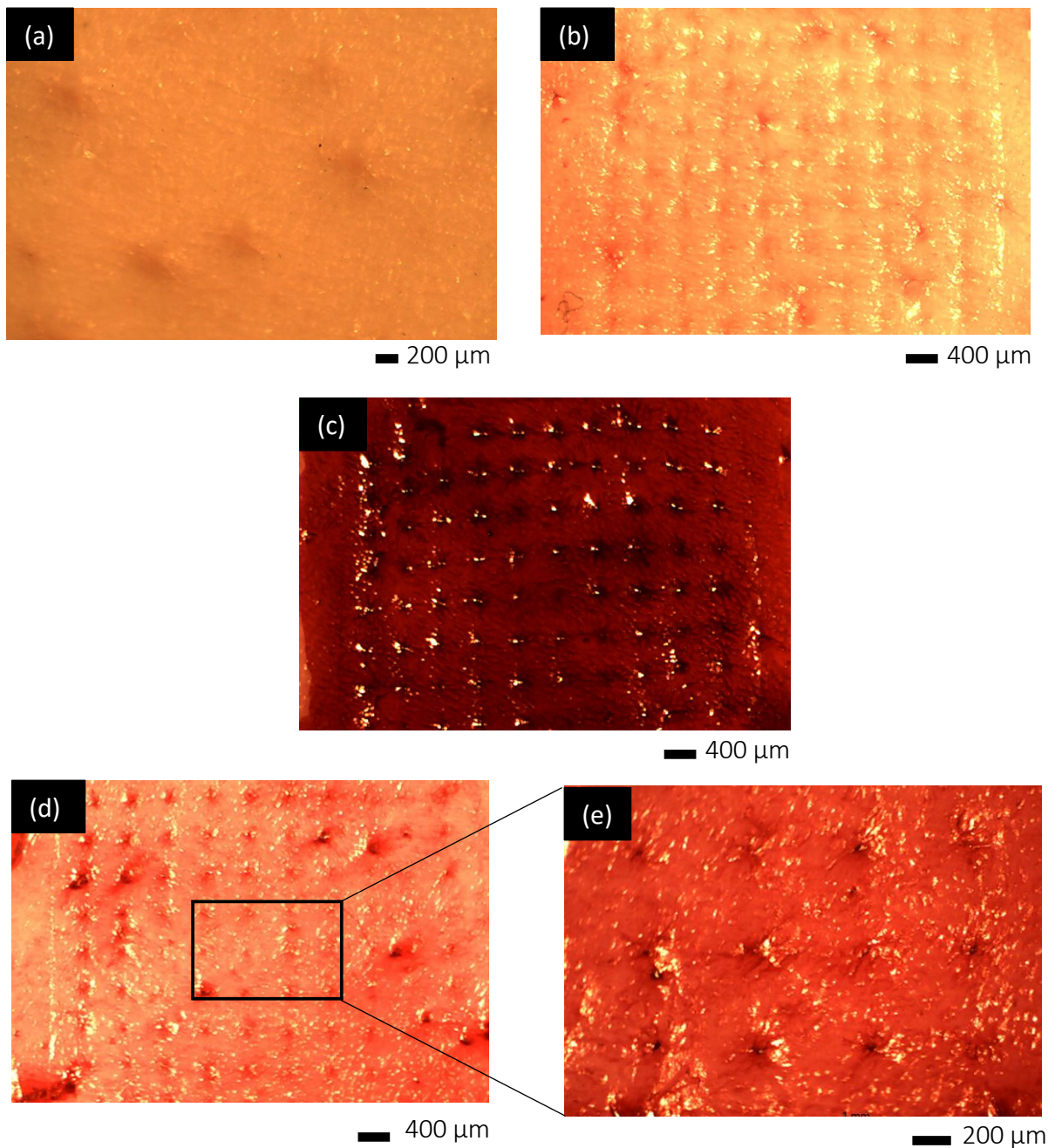
Figure 4.16. Insertion of 10×10, 0.75% CNC microneedles into pig skin tissue. (a) Pig skin before insertion of the microneedles, (b) Pig skin after insertion of microneedles, (c) after staining tissue marking dye, and (d, e) after cleaning- the unreacted dye on the skin surface.

4.6. Discussion

A novel microneedle formulation with CNC was proven to exhibit good mechanical strength in this work. There have been several studies and research done to fabricate polymeric microneedles for transdermal applications [92,93,24], however the main concerning factors are mechanical strength and long-term stability of microneedles. The mechanical strengths of the fabricated polymeric and sugar-based needles are not strong enough to penetrate the skin [101]. To overcome these challenges, we proposed an idea of CNC microneedles with a protection coating. Compared to microneedles made of sugar + CMC formulation, CNC microneedles exhibited 7-fold higher mechanical strength. The compatibility of CNC with biopharmaceuticals has not yet tested in this work. However, it was observed that the microneedles with 0.75% (w/w) CNC showed 3-fold higher failure force than the force required for insertion into the pig skin. Furthermore, CNC microneedles with a protection coating using anionic copolymer were proven to increase mechanical strength of the microneedles. Importantly, the long-term stability under controlled environmental conditions have not been investigated yet. As such, we would further perform long term stability tests using drug/vaccine-encapsulated microneedles to further evaluate the performance of the CNC microneedles with a protective coating. In spite of the need of further research, we believe that CNC microneedles coated with a protection layer could resolve major technical challenges for general application of microneedle technology to humans and animals.

5. Conclusion and Future work

In this work, we have demonstrated that pH-sensitive anionic copolymer can be used to solve technical problems in developing universal oral and transdermal drug delivery systems. To this end, we were able to synthesize anionic pH-sensitive copolymers by free radical polymerisation with different pKa values, which could be used for developing intestine-targeted oral drug formulations based on the microparticles with pH-responsive macropores. We were also able to develop CNC-incorporated microneedles with a protective anionic copolymer coating, which were proven to increase mechanical strength. This can enable the development of universal transdermal drug delivery systems, which can be even applicable to animals with thicker and stronger skins. Lastly, for successful implementation of current project, the following research must be performed in the future.

A. Anionic copolymer microparticles with a pH-responsive macropore

- Encapsulation of Influenza vaccine

- Pore closure- mechanism studies

- Vaccine preservation and environmental/long-term stability tests with formulations

- *In vivo* drug release mechanisms

- Long-term storage stability tests

B. Anionic copolymer-coated microneedles

- Pig skin penetration tests

- Time-dependent release of FNPs and real drugs depending on the type and source of tissues

- Influenza vaccine encapsulation and release tests

- Vaccine stability with CNC formulations

- Environmental/Long-term storage stability tests

6. References

[1]   Tiwari, G., Tiwari, R., Sriwastawa, B., Bhati, L., Pandey, S., Pandey, P., & Bannerjee, S. K. (2012). Drug delivery systems: An updated review. International journal of pharmaceutical investigation, 2(1), 2.

[2]   Gupta, P., Vermani, K., & Garg, S. (2002). Hydrogels: from controlled release to pH-responsive drug delivery. Drug discovery today, 7(10), 569-579.

[3]   Hassan, B. R. (2012). Overview on drug delivery system. Pharm Anal Acta, 3(10).

[4]   Alatorre-Meda, M., Alvarez-Lorenzo, C., Concheiro, A., & Taboada, P. (2013). UV and near-IR triggered release from polymeric micelles and nanoparticles. Smart materials for drug delivery, 1, 304.

[5]   Wang, N. X., & von Recum, H. A. (2011). Affinity-based drug delivery. Macromolecular bioscience, 11(3), 321-332.

[6]   "Common Routes of Drug Administration". Intro to Pharmacology. Eugene, Oregon: Lane Community College. Retrieved 2018-10-04.

[7]   "The administration of medicines". Nursing Times. https://www.nursingtimes.net/clinical-archive/medicine-management/the-administration-of-medicines-19-11-2007/ 2007-11-19. Retrieved 2018-10-04.

[8]   Bertrand, N., & Leroux, J. C. (2012). The journey of a drug-carrier in the body: an anatomo-physiological perspective. Journal of controlled release, 161(2), 152-163.

[9]   Ensign, L. M., Cone, R., & Hanes, J. (2012). Oral drug delivery with polymeric nanoparticles: the gastrointestinal mucus barriers. Advanced drug delivery reviews, 64(6), 557-570.

[10] Schmaljohann, D. (2006). Thermo-and pH-responsive polymers in drug delivery. Advanced drug delivery reviews, 58(15), 1655-1670.

[11] Huh, K. M., Kang, H. C., Lee, Y. J., & Bae, Y. H. (2012). pH-sensitive polymers for drug delivery. Macromolecular research, 20(3), 224-233.

[12] Tzeng, S. Y., Guarecuco, R., McHugh, K. J., Rose, S., Rosenberg, E. M., Zeng, Y., ... & Jaklenec, A. (2016). Thermostabilization of inactivated polio vaccine in PLGA-based microspheres for pulsatile release. Journal of controlled release, 233, 101-113.

[13] Pastore, M. N., Kalia, Y. N., Horstmann, M., & Roberts, M. S. (2015). Transdermal patches: history, development and pharmacology. British journal of pharmacology, 172(9), 2179-2209.

[14] Amato, D. V., Lee, H., Werner, J. G., Weitz, D. A., & Patton, D. L. (2017). Functional Microcapsules via Thiol–Ene Photopolymerization in Droplet-Based Microfluidics. ACS applied materials & interfaces, 9(4), 3288-3293.

[15] Amstad, E., Spaepen, F., Brenner, M. P., & Weitz, D. A. (2017). The microfluidic nebulator: production of sub-micrometer sized airborne drops. Lab on a Chip, 17(8), 1475-1480.

[16] Homayun, B., Sun, C., Kumar, A., Montemagno, C., & Choi, H. J. (2018). Facile fabrication of microparticles with pH-responsive macropores for small intestine targeted drug formulation. European Journal of Pharmaceutics and Biopharmaceutics, 128, 316-326.

[17] https://www.sigmaaldrich.com/content/dam/sigma-aldrich/docs/Aldrich/General_Information/thermal_initiators.pdf?utm_source=redirect&utm_medium=promotional&utm_campaign=insite_thermal_initiators.

[18]   Jeong, B., & Gutowska, A. (2002). Lessons from nature: stimuli-responsive polymers and their biomedical applications. TRENDS in Biotechnology, 20(7), 305-311.

[19]   Nielsen, L. H., Rades, T., Boyd, B., & Boisen, A. (2017). Microcontainers as an oral delivery system for spray dried cubosomes containing ovalbumin. European Journal of Pharmaceutics and Biopharmaceutics, 118, 13-20.

[20]   Amstad, E., Chen, X., Eggersdorfer, M., Cohen, N., Kodger, T. E., Ren, C. L., & Weitz, D. A. (2017). Parallelization of microfluidic flow-focusing devices. Physical Review E, 95(4), 043105.

[21]   Vo, A. Q., Feng, X., Morott, J. T., Pimparade, M. B., Tiwari, R. V., Zhang, F., & Repka, M. A. (2016). A novel floating controlled release drug delivery system prepared by hot-melt extrusion. European Journal of Pharmaceutics and Biopharmaceutics, 98, 108-121.

[22]   Davis, M., & Walker, G. (2018). Recent strategies in spray drying for the enhanced bioavailability of poorly water-soluble drugs. Journal of Controlled Release, 269, 110-127.

[23]   Mazutis, L., Vasiliauskas, R., & Weitz, D. A. (2015). Microfluidic production of alginate hydrogel particles for antibody encapsulation and release. Macromolecular bioscience, 15(12), 1641-1646.

[24]   Koch, B., Rubino, I., Quan, F. S., Yoo, B., & Choi, H. J. (2016). Microfabrication for drug delivery. Materials, 9(8), 646.

[25]   Kumar, A., Montemagno, C., & Choi, H. J. (2017). Smart microparticles with a pH-responsive macropore for targeted oral drug delivery. Scientific reports, 7(1), 3059.

[26]   Cheng, X., Liu, R., & He, Y. (2010). A simple method for the preparation of monodisperse protein-loaded microspheres with high encapsulation efficiencies. European Journal of Pharmaceutics and Biopharmaceutics, 76(3), 336-341.

[27]   Duncanson, W. J., Lin, T., Abate, A. R., Seiffert, S., Shah, R. K., & Weitz, D. A. (2012). Microfluidic synthesis of advanced microparticles for encapsulation and controlled release. Lab on a Chip, 12(12), 2135-2145.

[28]   Ramazani, F., Chen, W., van Nostrum, C. F., Storm, G., Kiessling, F., Lammers, T., ... & Kok, R. J. (2016). Strategies for encapsulation of small hydrophilic and amphiphilic drugs in PLGA microspheres: state-of-the-art and challenges. International journal of pharmaceutics, 499(1-2), 358-367.

[29]   Thakral, S., Thakral, N. K., & Majumdar, D. K. (2013). Eudragit®: a technology evaluation. Expert opinion on drug delivery, 10(1), 131-149.

[30]   Russell-Jones, G. J. (2000). Oral vaccine delivery. Journal of controlled release, 65(1-2), 49-54.

[31]   Wang, L., & Coppel, R. L. (2008). Oral vaccine delivery: can it protect against non-mucosal pathogens? Expert review of vaccines, 7(6), 729-738.

[32]   Silin, D. S., Lyubomska, O. V., Jirathitikal, V., & Bourinbaiar, A. S. (2007). Oral vaccination: where we are? Expert opinion on drug delivery, 4(4), 323-340.

[33]   Lavelle, E. C., & O'Hagan, D. T. (2006). Delivery systems and adjuvants for oral vaccines. Expert opinion on drug delivery, 3(6), 747-762.

[34]   Aziz, M. A., Midha, S., Waheed, S. M., & Bhatnagar, R. (2007). Oral vaccines: new needs, new possibilities. Bioessays, 29(6), 591-604.

[35]   O'Donnell, P. B., & McGinity, J. W. (1997). Preparation of microspheres by the solvent evaporation technique. Advanced drug delivery reviews, 28(1), 25-42.

[36]   Lawrence, M. J., & Rees, G. D. (2000). Microemulsion-based media as novel drug delivery systems. Advanced drug delivery reviews, 45(1), 89-121.

[37]   Freitas, S., Merkle, H. P., & Gander, B. (2005). Microencapsulation by solvent extraction/evaporation: reviewing the state of the art of microsphere preparation process technology. Journal of controlled release, 102(2), 313-332.

[38]   Li, M., Rouaud, O., & Poncelet, D. (2008). Microencapsulation by solvent evaporation: State of the art for process engineering approaches. International Journal of pharmaceutics, 363(1-2), 26-39.

[39]   Desai, U. R., & Klibanov, A. M. (1995). Assessing the structural integrity of a lyophilized protein in organic solvents. Journal of the American Chemical Society, 117(14), 3940-3945.

[40]   Maa, Y. F., & Hsu, C. C. (1997). Protein denaturation by combined effect of shear and air-liquid interface. Biotechnology and bioengineering, 54(6), 503-512.

[41]   Sah, H. (1999). Protein behavior at the water/methylene chloride interface. Journal of pharmaceutical sciences, 88(12), 1320-1325.

[42]   van de Weert, M., Hennink, W. E., & Jiskoot, W. (2000). Protein instability in poly (lactic-co-glycolic acid) microparticles. Pharmaceutical research, 17(10), 1159-1167.

[43]   van de Weert, M., Hoechstetter, J., Hennink, W. E., & Crommelin, D. J. (2000). The effect of a water/organic solvent interface on the structural stability of lysozyme. Journal of controlled release, 68(3), 351-359.

[44]   Prakadan, S. M., Shalek, A. K., & Weitz, D. A. (2017). Scaling by shrinking empowering single-cell'omics' with microfluidic devices. Nature Reviews Genetics, 18(6), 345.

[45]   De las Heras Alarcón, C., Pennadam, S., & Alexander, C. (2005). Stimuli responsive polymers for biomedical applications. Chemical Society Reviews, 34(3), 276-285.

[46]   Jeong, B., & Gutowska, A. (2002). Lessons from nature: stimuli-responsive polymers and their biomedical applications. TRENDS in Biotechnology, 20(7), 305-311.

[47]   https://www.who.int/influenza/spotlight.

[48]   Viswanathan, P., Muralidaran, Y., & Ragavan, G. (2017). Challenges in oral drug delivery: a nano-based strategy to overcome. In Nanostructures for Oral Medicine (pp. 173-201). Elsevier.

[49]   Dubé, M. A., Soares, J. B., Penlidis, A., & Hamielec, A. E. (1997). Mathematical modeling of multicomponent chain-growth polymerizations in batch, semibatch, and continuous reactors: a review. Industrial & Engineering Chemistry Research, 36(4), 966-1015.

[50]   Lin-Vien, D., Colthup, N. B., Fateley, W. G., & Grasselli, J. G. (1991). The handbook of infrared and Raman characteristic frequencies of organic molecules. Elsevier.

[51]   Giordanengo, R., Viel, S., Hidalgo, M., Allard-Breton, B., Thévand, A., & Charles, L. (2009). Structural characterization of a poly (methacrylic acid)–poly (methyl methacrylate) copolymer by nuclear magnetic resonance and mass spectrometry. Analytica chimica acta, 654(1), 49-58.

[52]   Brar, A. S., Singh, G., & Shankar, R. (2004). Structural investigations of poly (methyl methacrylate) by two-dimensional NMR. Journal of molecular structure, 703(1-3), 69-81.

[53]   Lyerla, J. R. (1977). NMR Study of the Chain Microstructure of P (MMA-co-MAA). IBM Journal of Research and Development, 21(2), 111-120.

[54]   Dai, S., Ravi, P., & Tam, K. C. (2008). pH-Responsive polymers: synthesis, properties and applications. Soft Matter, 4(3), 435-449.

[55] Yakimtsova, L. B., Egorova, E. L., Matusevich, Y. I., Selevich, K. A., & Kurtikova, A. L. (2009). Preparation and thermal degradation of methyl methacrylate-methacrylic acid copolymers. Russian Journal of Applied Chemistry, 82(9), 1636-1643.

[56] Smets, G., & Van Gorp, R. (1969). Acrylic and methacrylic acid copolymerization parameters. European Polymer Journal, 5(1), 15-19.

[57] Reed, W. F., & Alb, A. M. (2014). Monitoring polymerization reactions: from fundamentals to applications. John Wiley & Sons.

[58] Barroso, T., Temtem, M., Casimiro, T., & Aguiar-Ricardo, A. (2009). Development of pH-responsive poly (methylmethacrylate-co-methacrylic acid) membranes using scCO2 technology. Application to protein permeation. The Journal of Supercritical Fluids, 51(1), 57-66.

[59] Zhang, J., & Peppas, N. A. (2000). Synthesis and characterization of pH-and temperature-sensitive poly (methacrylic acid)/poly (N-isopropylacrylamide) interpenetrating polymeric networks. Macromolecules, 33(1), 102-107.

[60] Schenk, M., & Mueller, C. (2008). The mucosal immune system at the gastrointestinal barrier. Best Practice & Research Clinical Gastroenterology, 22(3), 391-409.

[61] Alexander, A., Dwivedi, S., Giri, T. K., Saraf, S., Saraf, S., & Tripathi, D. K. (2012). Approaches for breaking the barriers of drug permeation through transdermal drug delivery. Journal of Controlled Release, 164(1), 26-40.

[62] Paudel, K. S., Milewski, M., Swadley, C. L., Brogden, N. K., Ghosh, P., & Stinchcomb, A. L. (2010). Challenges and opportunities in dermal/transdermal delivery. Therapeutic delivery, 1(1), 109-131.

[63] Guy, R. H. (1989). Transdermal Drug Delivery. Ed. Hadgraft J, Guy RH.

[64]   Wester, R. C., & Maibach, H. I. (1995). Penetration enhancement by skin hydration. In Percutaneous Penetration Enhancers (p. 21). CRC Press Boca Raton, FL.

[65]   Amsden, B. G., & Goosen, M. F. A. (1995). Transdermal delivery of peptide and protein drugs: an overview. AIChE journal, 41(8), 1972-1997.

[66]   Magnusson, B. M., Walters, K. A., & Roberts, M. S. (2001). Veterinary drug delivery: potential for skin penetration enhancement. Advanced drug delivery reviews, 50(3), 205-227.

[67]   Lopez, R. F., Seto, J. E., Blankschtein, D., & Langer, R. (2011). Enhancing the transdermal delivery of rigid nanoparticles using the simultaneous application of ultrasound and sodium lauryl sulfate. Biomaterials, 32(3), 933-941.

[68]   Lai-Cheong, J. E., & McGrath, J. A. (2013). Structure and function of skin, hair and nails. Medicine, 41(6), 317-320.

[69]   Candi, E., Schmidt, R., & Melino, G. (2005). The cornified envelope: a model of cell death in the skin. Nature reviews Molecular cell biology, 6(4), 328.

[70]   Nir, Y., Paz, A., Sabo, E., & Potasman, I. (2003). Fear of injections in young adults: prevalence and associations. The American journal of tropical medicine and hygiene, 68(3), 341-344.

[71]   Henry, S., McAllister, D. V., Allen, M. G., & Prausnitz, M. R. (1998). Microfabricated microneedles: a novel approach to transdermal drug delivery. Journal of pharmaceutical sciences, 87(8), 922-925.

[72]   Prausnitz, M. R., Bose, V. G., Langer, R., & Weaver, J. C. (1993). Electroporation of mammalian skin: a mechanism to enhance transdermal drug delivery. Proceedings of the National Academy of Sciences, 90(22), 10504-10508.

[73] Mitragotri, S., Blankschtein, D., & Langer, R. (1995). Ultrasound-mediated transdermal protein delivery. Science, 269(5225), 850-853.

[74] Prausnitz, M. R., & Langer, R. (2008). Transdermal drug delivery. Nature biotechnology, 26(11), 1261.

[75] Adhikari, B. B., Goodson, J. L., Chu, S. Y., Rota, P. A., & Meltzer, M. I. (2016). Assessing the potential cost-effectiveness of microneedle patches in childhood measles vaccination programs: the case for further research and development. Drugs in R&D, 16(4), 327-338.

[76] Kim, Y. C., Park, J. H., & Prausnitz, M. R. (2012). Microneedles for drug and vaccine delivery. Advanced drug delivery reviews, 64(14), 1547-1568.

[77] Kalia, Y. N., Naik, A., Garrison, J., & Guy, R. H. (2004). Iontophoretic drug delivery. Advanced drug delivery reviews, 56(5), 619-658.

[78] Polat, B. E., Blankschtein, D., & Langer, R. (2010). Low-frequency sonophoresis: application to the transdermal delivery of macromolecules and hydrophilic drugs. Expert opinion on drug delivery, 7(12), 1415-1432.

[79] A Charoo, N., Rahman, Z., A Repka, M., & N Murthy, S. (2010). Electroporation: an avenue for transdermal drug delivery. Current drug delivery, 7(2), 125-136.

[80] Lim, D. J., Vines, J. B., Park, H., & Lee, S. H. (2018). Microneedles: a versatile strategy for transdermal delivery of biological molecules. International journal of biological macromolecules, 110, 30-38.

[81] Cheung, K., & Das, D. B. (2016). Microneedles for drug delivery: trends and progress. Drug delivery, 23(7), 2338-2354.

[82] Ritchie, Hannah, and Max Roser. "Meat and Dairy Production." Our World in Data (2017).

[83] https://www.foodunfolded.com/how-it-works/animal-vaccination-meat-safety.

[84]   http://www.fao.org/ag/againfo/resources/documents/AH/GREP_flyer.pdf.

[85]   Scudamore, J. M. (2007). Consumer attitudes to vaccination of food-producing animals. Revue scientifique et technique-Office international des épizooties, 26(2), 451.

[86]   Ramirez, A. (2018). Diseases affecting pigs: an overview of common bacterial, viral and parasitic pathogens of pigs.

[87]   Nelson, M. I., & Vincent, A. L. (2015). Reverse zoonosis of influenza to swine: new perspectives on the human–animal interface. Trends in microbiology, 23(3), 142-153.

[88]   Vincent, A., Awada, L., Brown, I., Chen, H., Claes, F., Dauphin, G., ... & Mumford, E. (2014). Review of influenza A virus in swine worldwide: a call for increased surveillance and research. Zoonoses and public health, 61(1), 4-17.

[89]   Larraneta, E., Lutton, R. E., Woolfson, A. D., & Donnelly, R. F. (2016). Microneedle arrays as transdermal and intradermal drug delivery systems: materials science, manufacture and commercial development. Materials Science and Engineering: R: Reports, 104, 1-32.

[90]   Miyano, T., Tobinaga, Y., Kanno, T., Matsuzaki, Y., Takeda, H., Wakui, M., & Hanada, K. (2005). Sugar micro needles as transdermic drug delivery system. Biomedical Microdevices, 7(3), 185-188.

[91]   Choi, H. J., Bondy, B. J., Yoo, D. G., Compans, R. W., Kang, S. M., & Prausnitz, M. R. (2013). Stability of whole inactivated influenza virus vaccine during coating onto metal microneedles. Journal of controlled release, 166(2), 159-171.

[92]   Donnelly, R. F., Singh, T. R. R., & Woolfson, A. D. (2010). Microneedle-based drug delivery systems: microfabrication, drug delivery, and safety. Drug delivery, 17(4), 187-207.

[93] Park, J. H., Allen, M. G., & Prausnitz, M. R. (2005). Biodegradable polymer microneedles: fabrication, mechanics and transdermal drug delivery. Journal of controlled release, 104(1), 51-66.

[94] Donnelly, R. F., Singh, T. R. R., Morrow, D. I., & Woolfson, A. D. (2012). Microneedle-mediated transdermal and intradermal drug delivery. John Wiley & Sons.

[95] Choi, H. J., Yoo, D. G., Bondy, B. J., Quan, F. S., Compans, R. W., Kang, S. M., & Prausnitz, M. R. (2012). Stability of influenza vaccine coated onto microneedles. Biomaterials, 33(14), 3756-3769.

[96] Whitfield, R., Truong, N. P., Messmer, D., Parkatzidis, K., Rolland, M., & Anastasaki, A. (2019). Tailoring polymer dispersity and shape of molecular weight distributions: methods and applications. Chemical Science, 10(38), 8724-8734.

[97] Kim, Y. C., Quan, F. S., Compans, R. W., Kang, S. M., & Prausnitz, M. R. (2010). Formulation and coating of microneedles with inactivated influenza virus to improve vaccine stability and immunogenicity. Journal of controlled release, 142(2), 187-195.

[98] Keith, A. D. (1983). Polymer matrix considerations for transdermal devices. Drug development and industrial pharmacy, 9(4), 605-625.

[99] Raphael, A. P., Crichton, M. L., Falconer, R. J., Meliga, S., Chen, X., Fernando, G. J., ... & Kendall, M. A. (2016). Formulations for microprojection/microneedle vaccine delivery: structure, strength and release profiles. Journal of controlled release, 225, 40-52.

[100] Wu, F., Yang, S., Yuan, W., & Jin, T. (2012). Challenges and strategies in developing microneedle patches for transdermal delivery of protein and peptide therapeutics. Current pharmaceutical biotechnology, 13(7), 1292-1298.

[101]   Hong, X., Wei, L., Wu, F., Wu, Z., Chen, L., Liu, Z., & Yuan, W. (2013). Dissolving and biodegradable microneedle technologies for transdermal sustained delivery of drug and vaccine. Drug design, development and therapy, 7, 945.

[102]   Homayun, B., Kumar, A., Nascimento, P. T., & Choi, H. J. (2018). Macropored microparticles with a core–shell architecture for oral delivery of biopharmaceuticals. Archives of pharmacal research, 41(8), 848-860.

[103]   Homayun, B., Lin, X., & Choi, H. J. (2019). Challenges and Recent Progress in Oral Drug Delivery Systems for Biopharmaceuticals. Pharmaceutics, 11(3), 129.

[104]   Lahiji, S. F., Kim, Y., Kang, G., Kim, S., Lee, S., & Jung, H. (2019). Tissue Interlocking Dissolving Microneedles for Accurate and Efficient Transdermal Delivery of Biomolecules. Scientific reports, 9(1), 1-9.

[105]   Lee, J. W., Park, J. H., & Prausnitz, M. R. (2008). Dissolving microneedles for transdermal drug delivery. Biomaterials, 29(13), 2113-2124.